Atmos. Chem. Phys., 13, 11551–11571, 2013
www.atmos-chem-phys.net/13/11551/2013/
doi:10.5194/acp-13-11551-2013

Atmospheric Chemistry and Physics Open Access

Secondary organic aerosol formation and primary organic aerosol oxidation from biomass-burning smoke in a flow reactor during FLAME-3

A. M. Ortega[1,2], **D. A. Day**[1,3], **M. J. Cubison**[1,3,*], **W. H. Brune**[4], **D. Bon**[1,3,5,**], **J. A. de Gouw**[1,5], **and J. L. Jimenez**[1,3]

[1]Cooperative Institute for Research in the Environmental Sciences, University of Colorado, Boulder, CO, USA
[2]Department of Atmospheric and Oceanic Sciences, University of Colorado, Boulder, CO, USA
[3]Department of Chemistry and Biochemistry, University of Colorado, Boulder, CO, USA
[4]Department of Meteorology, Pennsylvania State University, University Park, PA, USA
[5]Chemical Sciences Division, NOAA Earth System Research Laboratory, Boulder, CO, USA
[*]now at: Tofwerk AG, Thun, Switzerland
[**]now at: Planning and Policy Program, Air Pollution Control Division, Colorado Department of Public Health and Environment, Denver, CO, USA

Received: 19 April 2013 – Published in Atmos. Chem. Phys. Discuss.: 23 May 2013
Revised: 16 September 2013 – Accepted: 23 September 2013 – Published: 28 November 2013

Abstract. We report the physical and chemical effects of photochemically aging dilute biomass-burning smoke. A "potential aerosol mass" (PAM) flow reactor was used with analysis by a high-resolution aerosol mass spectrometer and a proton-transfer-reaction ion-trap mass spectrometer during the FLAME-3 campaign. Hydroxyl (OH) radical concentrations in the reactor reached up to ∼ 1000 times average tropospheric levels, producing effective OH exposures equivalent to up to 5 days of aging in the atmosphere, and allowing for us to extend the investigation of smoke aging beyond the oxidation levels achieved in traditional smog chambers. Volatile organic compound (VOC) observations show aromatics and terpenes decrease with aging, while formic acid and other unidentified oxidation products increase. Unidentified gas-phase oxidation products, previously observed in atmospheric and laboratory measurements, were observed here, including evidence of multiple generations of photochemistry. Substantial new organic aerosol (OA) mass ("net SOA"; secondary OA) was observed from aging biomass-burning smoke, resulting in total OA average of 1.42 ± 0.36 times the initial primary OA (POA) after oxidation. This study confirms that the net-SOA-to-POA ratio of biomass-burning smoke is far lower on average than that observed for urban emissions. Although most fuels were very reproducible, significant differences were observed among the biomasses, with some fuels resulting in a doubling of the OA mass, while for others a very small increase or even a decrease was observed. Net SOA formation in the photochemical reactor increased with OH exposure (OH_{exp}), typically peaking around three days of equivalent atmospheric photochemical age ($OH_{exp} \sim 3.9 \times 10^{11}$ molecules cm^{-3} s), then leveling off at higher exposures. The amount of additional OA mass added from aging is positively correlated with initial POA concentration, but not with the total VOC concentration or the concentration of known SOA precursors. The mass of SOA formed often exceeded the mass of the known VOC precursors, indicating the likely importance of primary semivolatile/intermediate volatility species, and possibly of unidentified VOCs as SOA precursors in biomass burning smoke. Chemical transformations continued even after mass concentration stabilized. Changes in the biomass-burning tracer f_{60} ranged from substantially decreasing to remaining constant with increased aging. With increased OH_{exp}, oxidation was always detected (as indicated by f_{44} and O / C). POA O / C ranged from 0.15 to 0.5, while aged OA O / C reached up to 0.87. The rate of oxidation and maximum O / C achieved differs for each biomass, and appears to increase with the initial O / C of the POA.

Published by Copernicus Publications on behalf of the European Geosciences Union.

1 Introduction

Atmospheric aerosols – liquid droplets or solid particles suspended in air – have significant influence on the radiative forcing of climate (Forster et al., 2007), human health (Pope et al., 2002), regional visibility (Watson, 2002), and deposition of acids, toxins, and nutrients on ecosystems and crops (Matson et al., 2002). These impacts depend on the aerosol particle concentration, size distribution, and chemical composition. Organic aerosols (OA) represent a substantial fraction (20–90 %) of total submicron aerosol mass (Zhang et al., 2007; Murphy et al., 2006). OA is the most diverse and least understood component of submicron aerosols, in part because of a wide variety of biogenic and anthropogenic sources as well as contributions from both direct emission and secondary formation in the atmosphere (Jimenez et al., 2009). OA is either emitted directly into the atmosphere from such sources as forest fires and transportation as primary organic aerosol (POA) or is formed in the atmosphere from photochemical and aqueous reactions as secondary organic aerosol (SOA). Developing a full understanding of the sources, atmospheric processes, and chemical properties of OA is essential to constraining and predicting its impacts on human health and climate, as well as how these impacts may be altered with changing climate and emissions patterns (Hallquist et al., 2009).

Regional ambient aerosol levels can be significantly enhanced by smoke emitted from prescribed burns and wildfires over many seasons and locations (Park et al., 2007; Spracklen et al., 2007). The use of wood as a fuel for heating also increases aerosol levels (Alfarra et al., 2007). Biomass burning can severely influence local and regional air quality, and is a major global source of trace gases and aerosols (McMeeking et al., 2009; de Gouw and Jimenez, 2009). Understanding the photochemical evolution of biomass-burning OA (BBOA) and volatile organic compound (VOC) emissions when they undergo atmospheric aging is crucial to obtaining a more complete picture of biomass-burning effects in the atmosphere and developing better estimates of biomass-burning impacts in regional and global models.

A number of laboratory experiments and field projects have examined biomass-burning emissions and contributions to overall OA mass. While BBOA is emitted as POA, recent field studies indicate BBOA emissions are semivolatile and can evaporate upon dilution of a smoke plume (Robinson et al., 2007). SOA can also form from biomass-burning VOCs or evaporated POA species. We will refer to the excess mass formed during photochemical aging over the initial POA as "net SOA." As defined here, net SOA may be positive if SOA formation exceeds POA losses or negative if the opposite is true. Some studies examining photochemical processing of wood smoke indicate production of substantial production of SOA, which was attributed to mostly gas-phase reactions from semivolatile and intermediate volatility species (S/IVOCs) (Grieshop et al., 2009; Hennigan et al., 2011). Estimates of net SOA from field studies range from a small decrease or no change in mass over the initial POA (Capes et al., 2008; Cubison et al., 2011; Hecobian et al., 2011; Akagi et al., 2012; Jolleys et al., 2012) to net SOA equal to a substantial fraction of the initial POA mass (Yokelson et al., 2009; DeCarlo et al., 2010). OA mass loss from secondary processing (including aging and evolution of an airmass) has been explained by evaporation upon dilution (Robinson et al., 2007), heterogeneous oxidation leading to fragmentation reactions increasing volatility of reaction products (Lambe et al., 2012; Molina et al., 2004), and gas-phase oxidation and fragmentation leading to evaporation of particle-phase semivolatiles that were in equilibrium with the gas-phase species before the latter reacted and fragmented (Donahue et al., 2012).

Quantification of net SOA formation and aging from biomass-burning smoke in the field is thus confounded by substantial variability between studies, which may be due to the different gas and particle-phase emissions due to variations in fuel type and burning conditions – such as flaming or smoldering (Koppmann et al., 1997) – or the environment where the smoke is emitted (Akagi et al., 2012). Laboratory studies of aging of biomass burning can play an important role in elucidating the importance of different factors in smoke aging.

To date, such studies have only been performed with large ($\sim 10\,m^3$ or larger) environmental chambers (Hennigan et al., 2011; Grieshop et al., 2009).While large environmental chambers have the advantage of using similar oxidant levels as in the atmosphere, such chambers can typically only be used for one experiment per day, and can suffer from wall loses of semivolatiles and particles to walls (Matsunaga and Ziemann, 2010). An experimental technique is needed to characterize the SOA-formation potential of biomass-burning emissions that is capable of rapid operation to allow for examining variability of smoke markers and different fuel types, and that responds in real time to changes in smoke composition during emission.

A "potential aerosol mass" (PAM) flow reactor, developed by Kang et al. (2007, 2011), is a small flow-through reactor that exposes samples to high oxidant levels with a short residence time. Recent work with the PAM reactor has examined SOA yield, oxidation, and chemical changes using single precursors or simple mixtures and has produced results similar to flow-tube and environmental chamber experiments with the same precursors (Lambe et al., 2011a, b; Kang et al., 2007, 2011). Compared to the Caltech Indoor Chamber Facility (Cocker et al., 2001; Keywood et al., 2004), at similar hydroxyl radical (OH) exposures, SOA from the PAM reactor was more oxidized than chamber SOA; some precursor yields were comparable (e.g., α-pinene), while other (e.g., *m*-xylene) yields were lower in the reactor than the Caltech chamber (Lambe et al., 2011a). OH oxidation of alkane SOA precursors in the reactor shows the effect of functionalization (oxygen addition) and fragmentation (carbon loss) reactions

in the absence of NO_x (Lambe et al., 2012). Also, oxygen-to-carbon (O / C) ratios from reactor oxidation result in a wider range than previously observed in the large chambers, due to higher levels of OH exposure. (Lambe et al., 2011b; Massoli et al., 2010). These studies show that the PAM reactor produces OA with characteristics similar to those of atmospheric OA (Bahreini et al., 2012).

In this study, we photochemically aged smoke from fuels combusted during a biomass-burning study (FLAME-3) at the US Department of Agriculture Fire Sciences Laboratory (FSL) at Missoula, Montana, during the period September–October 2009. We used a PAM flow reactor and monitored the effect of aging with submicron aerosol and gas-phase composition measurements. We present results from multiple biomasses that show the physical and chemical effects of OA aging and net SOA formation from aging biomass-burning smoke. Our work expands upon the previous literature by using the PAM reactor to study a complex system, biomass-burning smoke, in real time.

2 Methods

2.1 FLAME-3 experiment

Experiments with different types of biomass were conducted in the fire chamber at the US Department of Agriculture FSL in a "chamber burn" configuration, in which known quantities of biomass were burned openly to their natural extinction (McMeeking et al., 2009, as shown in Fig. S1a; Yokelson et al., 1996; Christian et al., 2003). Between 0.1 and 1 kg of fuel was placed on top of a ceramic plate and ignited by heating coils treated with a small amount of ethanol (Hennigan et al., 2011). The smoke from the fire filled the entire $\sim 3000\,m^3$ chamber, and was mixed throughout the chamber by large fans. Multiple gas and aerosol measurements indicated that the smoke was well mixed approximately 15 min after the fire extinguished itself. The initial dilution factor estimated from CO_2 concentrations was approximately 500. Smoke was held in the fire chamber for typically 3.5 h. Slow dilution with ambient air continued during the containment of the smoke because the fire chamber was not completely airtight. Typical ambient outdoor OA concentrations were low (a few $\mu g\,m^{-3}$) and did not significantly perturb the chamber OA that was present at much higher concentrations during this slow dilution. The use of the "chamber burn" configuration in the FSL fire chamber prohibited distinguishing between flaming- and smoldering phases of combustion. Modified combustion efficiency (MCE) and dilution/emission ratios to CO are not presented here due to lack high-quality CO measurements in this study. We also examined the relationship between organic aerosol enhancement and NO_x concentrations, but found no significant correlation. Conditions inside the chamber were stable with average relative humidity of $30.2 \pm 6.5\,\%$ (mean $\pm 1\sigma$) ranging from 18.2 to 42.9 %, and average temperature of $17.2 \pm 2.6\,°C$ ranging from 11.1 to 20.3 °C.

FLAME-3 was a targeted investigation of emissions from burning of plant species that are relevant to North American local and regional air quality and often undergo prescribed and wildfire burning (Hennigan et al., 2011). Species used as fuels included chaparral (ceanothus, chamise, and manzanita), pines (lodgepole and ponderosa pine), leafy and desert shrubs (gallberry, turkey oak, and sage), grasses (saw grass, wheat grass, wheat straw, and pocosin), spruces (white and black spruce), and soils (peat and Alaskan duff). In this work, we present data from 16 unique biomasses, used as fuels for 25 different chamber burns, as detailed in Table 1.

2.2 PAM flow reactor

To study the effect of photochemical aging on biomass-burning smoke, a PAM flow reactor was used to expose smoke to high levels of OH and O_3 with reduced wall losses and short response time. The reactor is a small (13.1 L) flow-through cylindrical vessel. The flow rate through the reactor was $4.4\,L\,min^{-1}$, resulting in an average residence time of approximately 180 s. The reactor is made of conductive aluminum, which eliminates the loss of charged particles due to charge build-up on walls made of insulating material such as glass or Teflon; using a Pyrex reactor in prior experiments led to near complete loss of charged particles. This loss may not be an issue when particles are generated inside of the reactor by nucleation (Lambe et al., 2011b); however, a large fraction of particles emitted from combustion can be charged and would thus be lost to the walls. No correction was made for possible semivolatile losses to walls, as the short residence time and high aerosol surface area of our experiments are expected to limit that problem. Particle mass losses were very small as discussed below.

OH and O_3 are produced when UV light from two low-pressure mercury lamps (model no. 82-9304-03, BHK, Inc.) initiates O_2, H_2O, and O_3 photochemistry. The 185 nm light photolyzes O_2 to produce O_3, and H_2O to produce OH and HO_2, while the 254 nm light photolyzes O_3 to produce OH. Subsequent chemistry determines the concentrations of O_3, OH, and other chemical species. The lamps were mounted in Teflon sleeves and purged with N_2 to control their temperature and avoid lamp exposure to high oxidant concentrations. We use the term "aging" to refer to the combined effect of OH, O_3, and light exposure in the flow reactor, although calculations indicate that OH reactions dominate. The intensity of aging was controlled by adjusting the voltage supplied to power the lamps between 50 and 110 VAC, thus modulating the photon flux and consequently the quasi-steady-state oxidant concentrations in the reactor. Typical OH scanning operation is highlighted in Fig. S2, where indicators of changing lamp voltage are marked by calculated photochemical age; see Sect. 2.5 for details.

Table 1. Experimental results of each fuel from FLAME-3, with maximum (deviation from unity, $ER_{OA} = 1$) sustained 5 min average organic aerosol enhancement ratio (ER_{OA}) with associated OH exposure (OH_{exp}), maximum unprocessed OA mass concentration, and starting weight of the biomass mass fuel before combustion. In some experiments, the O_3 monitor malfunctioned, and thus OH_{exp} could not be estimated; however, OH in the reactor was always scanned using the same methodology described.

Burn Number[a]	Fuel	Max Unprocessed[b]	Max ER_{OA}[c]	OH_{exp}[d]	Fuel Weight[e]
39	Black Spruce	376	1.33	3.16×10^{11}	250
40	Ponderosa Pine	12361	0.62	4.03×10^{11}	250
41	Pocosin	441	1.44	4.36×10^{11}	400
42	Wire Grass	1057	1.67	5.70×10^{11}	600
43	Saw Grass	604	1.51		350
44	Gallberry	3175	1.25		500
45	Turkey Oak	522	1.81	4.79×10^{11}	400
46	Wheat Straw	853	1.93	3.91×10^{11}	500
47	Gallberry	3235	1.24		500
48	Ponderosa Pine	7234	1.03		200
49	Sage	246	2.33	3.07×10^{11}	300
50	Lodgepole Pine	6975	0.9	2.05×10^{11}	150
51	Alaskan Duff	1629	1.23	4.31×10^{11}	200
52	Turkey Oak	10251	1.12	2.16×10^{11}	401
53	Sage	216	1.87		300
54	Manzanita	402	1.52		500
55	White spruce	2799	1.73	2.79×10^{11}	346
56	Wire grass	6321	1.36	2.34×10^{11}	500
58	Saw grass	9373	1.24	2.16×10^{11}	525
59	Chamise	231	1.93	1.95×10^{11}	500
60	Manzanita	329	1.57	2.00×10^{11}	502
61	Lodgepole Pine	18071	0.86	2.61×10^{11}	203
62	Ceanothus	2958	1.54	2.50×10^{11}	1002
63	Pocosin	2998	1.39		799
64	Peat	3665	1.1		344

[a] Number convention used during FLAME-3, [b] in units of $\mu g\,m^{-3}$ (at ambient temperature and pressure), [c] organic aerosol enhancement ratio (EROA = aged/unprocessed), [d] in units of molec. cm^{-3} s, [e] in units of grams (g).

While 185 nm UV light photochemically produces both OH and O_3, the OH/O_3 ratio in the reactor is about 10 times daytime ambient levels. In this study, OH exposure ranged from 1.36×10^{10} to 6.5×10^{11} molec. cm^{-3} s, and O_3 exposure from 1.5×10^{15} to 3.4×10^{16} molec. cm^{-3} s. Precursor reaction rates with OH are much faster than for O_3 for typical ambient OH and O_3 concentrations, with the exception of some olefinic biogenic VOC (BVOC) that can be comparable, i.e., ranging from 10 times faster to slower (Atkinson and Arey, 2003). The UV light could affect some organic species, such as organic peroxides, aldehydes, or aromatics that can be photolyzed by these wavelengths. However, for the estimated maximum photon fluxes in the reactor of 2×10^{13} photons $cm^{-2}\,s^{-1}$ at 185 nm and 2×10^{14} photons $cm^{-2}\,s^{-1}$ at 254 nm, photolysis of nonaromatic peroxides and aldehydes should be less than < 10 % (typically much less, with cross sections, σ, at 254 nm, ranging from 1.6 to 8×10^{-20} cm^2 molec.$^{-1}$), while some substituted aromatics (e.g., phenol, benzaldehyde, and *m*-, *o*-cresol, with $\sigma \sim 1.5 \times 10$–$17$ cm^2 molec.$^{-1}$, 1.41×10–18 cm^2 molec.$^{-1}$, and 1.2–1.6×10–17 cm^2 molec.$^{-1}$, respectively, at 254 nm) could photolyze as much as 50–90 % during the residence time in the reactor (Trost et al., 1997; Keller-Rudek and Moortgat, last access: 7 March 2013). However, reactions with the OH concentrations produced with these photon fluxes are more than 10 times faster than photolysis so that the dominant reaction pathway is with OH.

2.3 Instrumentation

Smoke-laden air from the fire chamber was continuously sampled through the flow reactor in an open-flow-through configuration via a 14 cm opening (Fig. S1b). Use of any inlet, including passivated SILCO steel, resulted in substantially reduced SOA formation, presumably because of loss of semivolatiles to the inlet and front plate of the reactor. For this reason, the reactor was located inside the FSL fire chamber. Reactor output was measured by an Aerodyne high-resolution time-of-flight aerosol mass spectrometer (HR-ToF-AMS – hereafter AMS; DeCarlo et al., 2006), O_3 monitor (2B Technologies, Model 205) and for selected

burns, a proton-transfer-reaction ion-trap mass spectrometer (PIT-MS; Warneke et al., 2005a, b). A copper bypass line was used to sample unprocessed smoke directly from the fire chamber, as shown in Fig. 1. During measurements, two valves were automatically switched, alternating sampling between the reactor and the bypass line with 1 min time resolution, and with sufficient instrument delays to avoid averaging of data from the previous phase that was still present on the lines after valve switching. This strategy allowed for near-continuous measurements of both OA produced by the fire (hereafter referred to as POA interchangeably with "unprocessed") and OA aged in the flow reactor.

The AMS measures submicron nonrefractory particles that evaporate in a few seconds or less at 600 °C in a high vacuum. Smoke was transported from the flow reactor to the AMS through a 3 m long insulated-copper inlet. Detailed information on the AMS can be found elsewhere (DeCarlo et al., 2006). AMS measurements were obtained using the "W" mode ion path, which offers higher mass resolution with a trade-off of a lower signal-to-noise ratio. Mass resolving power ($m/\Delta m$) was ~ 3400 at mass-to-charge (m/z) 200 in W mode. In this study, concentrations of the fresh smoke emissions were high enough to maintain an adequate signal-to-noise ratio in this mode. Data were averaged in 1 min intervals. All data were analyzed using standard AMS software (SQUIRREL v1.50-1.52F and PIKA v1.09-1.11G; Sueper et al., 2007) within Igor Pro 6.21–6.31 (WaveMetrics, Lake Oswego, OR). Although the AMS samples particles 10^7 times more efficiently than gases (Cubison et al., 2011; Canagaratna et al., 2007), levels of CO_2 were high and variable enough to affect the AMS measurements. The influence of CO_2 on the AMS measurements was removed by both a standard particle filter interpolation method and applying a time series of gas-phase CO_2 measurements (LI-COR Biosciences LI-6262 CO_2 / H_2O analyzer). A procedure was developed to correctly calculate sulfate and organic concentrations for biomass-burning smoke, since the standard AMS unit mass resolution (UMR) "fragmentation table" (Allan et al., 2004) does not work well for very high OA fractions of the total nonrefractory aerosols (Fig. S3 and Table S1).

High-resolution (HR) mass concentrations were calculated using the HR AMS fragmentation table, detailed in Aiken et al. (2008, 2007). Typical for biomass-burning smoke (e.g., DeCarlo et al., 2008), one-quarter of organic mass was above m/z 100, as indicated by a slope of 1.33 in Fig. S4a, where UMR organic mass concentration calculated from the full range of m/z is plotted with respect to HR data as calculated up to m/z 100. OA mass concentrations reported in this study are the combined mass of HR data up to m/z 100 and UMR above m/z 100, due to the difficulty of obtaining accurate information from the high-resolution fits at higher m/z, from the increasing number of different ions at each m/z and the limited resolution of the mass spectrometer.

The standard method of tracking changes in AMS sensitivity due to degradation of the microchannel plate (MCP) or

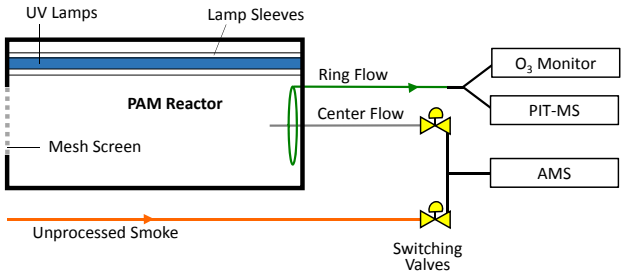

Fig. 1. Schematic of the potential aerosol mass (PAM) reactor coupled to an Aerodyne high-resolution time-of-flight aerosol mass spectrometer (AMS), proton-transfer-reaction ion-trap mass spectrometer (PIT-MS), and ozone (O_3) monitor. A copper bypass line (orange) allows for direct sampling of unprocessed smoke. Computer-controlled switching valves (yellow) alternate between AMS measurements from the flow reactor and the bypass line. Voltage supplied to UV lamps (blue) can be varied to control oxidant concentrations in the chamber. Ring flow (green) is a Teflon line and is used for gas-phase measurements; center flow (gray) is a stainless steel line that continuously extracts the sample for aerosol measurements.

changes in electron emission assumes an invariant nitrogen concentration in the sampled air, such that the measured signal at m/z 28, where N_2^+ is the dominant ion, linearly scales with instrument sensitivity. In this study, there was a substantial particle-phase signal at m/z 28 from the ions CO^+, $C_2H_4^+$, and CH_2N^+ (Fig. S5). Using high-resolution analysis techniques (DeCarlo et al., 2006; Sueper et al., 2007), N_2^+ signal was separated from the particle-phase signal at m/z 28, resulting in an N_2^+-only signal. This time series of the fitted N_2^+ ion peak area was used rather than the total integrated signal at m/z 28 as the "airbeam correction" (Allan et al., 2003). Grieshop et al. (2009) attributed the entire particle-phase signal at m/z 28 in wood smoke to CO^+ using a quadrupole AMS, but Fig. S5 shows that there can be substantial signals at $C_2H_4^+$ and CH_2N^+ as well. We examined the potential of using other m/z for tracking changes in AMS sensitivity (m/z 40 for Ar^+ and m/z 32 for O_2^+); however, due to high organic loadings in this study, all air m/z had substantial signal from organic ions present.

Quantification of ambient AMS measurements requires application of a collection efficiency (CE) to account for particle bounce at the AMS vaporizer (Canagaratna et al., 2007; Middlebrook et al., 2012). Typical values range from 0.5 to 1. For ambient aerosols, CE can be estimated from aerosol composition (Middlebrook et al., 2012); however, that parameterization does not always apply to laboratory studies, in particular when inorganic signals are very low relative to organic mass, such as in this study (Docherty et al., 2013). Since the focus of this study is on relative changes between directly emitted and aged smoke, AMS mass concentrations were calculated with a CE of 1. Two recent biomass-burning studies reported a CE of 1, supported by comparisons with Scanning

Mobility Particle Sizer (SMPS) measurements (Hennigan et al., 2011) and black carbon measurements (Heringa et al., 2011). The high levels of OA sampled in some of the burns are not thought to cause significant nonlinearity or other detection problems for the AMS, due to the low ion currents measured with the W mode and the short lifetime of the AMS OA background signal.

Elemental analysis was applied to AMS OA measurements to yield ratios of oxygen-to-carbon (O / C) and hydrogen-to-carbon (H / C) (Aiken et al., 2008). This calculation was performed with HR ion fits up to m/z 100, and implicitly assumes that the elemental composition of larger ions is similar to that of the ions below m/z 100. For the purpose of this study, nitrate, sulfate, ammonium, and chloride are assumed to be from inorganic sources; however, there may be some contribution to these nominally inorganic species from organic compounds (e.g., Farmer et al., 2010). The cation balance analysis – comparing the measured potassium (K^+) and ammonium (NH_4^+) to that predicted when considering sulfate, nitrate, and chloride as fully inorganic ions – indicates a deficit of cations (Fig. S4b). We have included K^+ (with a relative ionization efficiency of 2.9, Drewnick et al., 2006) in this balance because it is known to be an important cation in biomass-burning smoke (Lee et al., 2010). Na^+ was not included due to substantially lower concentrations than K^+ in biomass-burning smoke (McMeeking et al., 2009) as well as the difficulty of quantifying this ion with the AMS. The most likely explanation for the apparent cation deficit observed is inefficient detection by the AMS of K^+ or other mineral cations present in the smoke. It could also possibly have a contribution from organonitrates and/or organosulfates present in the smoke particles that would lead to too high estimates of inorganic nitrate or sulfate. However, we are not aware of reports of organonitrates or organosulfates in biomass-burning aerosols, and as such possible explanation remains speculative. Another possible reason for the observed cation deficit would be the presence of H^+ if the aerosols are acidic, since H^+ cannot be quantified directly by the AMS due to limitations of the time-of-flight mass spectrometer.

2.4 VOC measurement

A custom-built PIT-MS was deployed to quantify VOCs. Proton-transfer-reaction mass spectrometry (PTR-MS) has become a standard method for quantifying mixing ratios of common VOCs such as oxygenates, aromatics, and alkenes at ambient concentrations (de Gouw and Warneke, 2007). The PIT-MS instrument uses an ion source and drift-tube reactor identical to that of the commercial PTR-MS instrument but is equipped with a three-dimensional ion trap mass spectrometer instead of a quadrupole mass filter (Warneke et al., 2005a, b), allowing for detection of a full mass spectrum as opposed to a subset of specifically targeted compounds. During FLAME-3, the PIT-MS was used for simultaneous measurements of product ions with m/z 33–225, trapping times ranging from 0.5 to 2.0 s depending on VOC concentrations in the fire chamber. A 10 m long 1/8″ outside diameter Teflon line and a sample flow of 150 sccm were used to sample air from the fire chamber. Calibrations for 12 common VOCs, including toluene, were conducted using a gas standard before and after each burn throughout the experiment. Measurement uncertainty for the calibrated VOCs measured by PIT-MS was estimated to be ±30 %, and for the uncalibrated VOCs was estimated to be ∼50 %. A potential interference in benzene measurements (at m/z 79) due to water–acetic acid clusters appears to be negligible during FLAME-3 because of low relative humidity during the experiments.

2.5 Photochemical age estimation

OH exposure (OH_{exp}) is the integral of OH concentration and oxidation time. Typically, offline calibrations of OH exposure can be made by using the decay of SO_2 to reaction with OH at different UV light intensities, as described in Lambe et al. (2011a). For the conditions in our flow reactor, OH_{exp} can be modeled using measured O_3, RH, and flow rate:

$$OH_{exp} = [OH]\,\Delta t = \varepsilon \frac{[O_3]^{\alpha}\,[H_2O]^{\beta}}{\text{flow}}, \quad (1)$$

where $\varepsilon = 7.21 \times 10^{-7}$ (with OH_{exp} in units of molec cm^{-3} s when O_3 and H_2O are in units of molec cm^{-3} and the flow in L min^{-1}), $\alpha = 0.495$, and $\beta = 0.70$ are calibration parameters determined during offline SO_2 calibration; O_3 and H_2O are in units of molec. cm^{-3} and flow is in L min^{-1}. An equivalent "photochemical age" can be calculated by dividing this OH_{exp} by an assumed average atmospheric concentration of OH of 1.5×10^6 molecules cm^{-3} (Mao et al., 2009).

However, high concentrations of reactive VOCs can suppress OH by shifting OH to HO_2, thus reducing OH_{exp} (in a way not reflected in H_2O and O_3) so that the calibration equation no longer accurately describes OH_{exp}. In this study, sampling of biomass-burning smoke directly from the fire chamber resulted in very high concentrations of VOCs and POA, greater than 10^2 ppb VOCs and up to 10^4 µg m^{-3} POA. In order to test for possible OH suppression by this very reactive mixture, OH exposures were calculated from the online decay of toluene and benzene in the reactor during different OH concentrations (i.e. lamp intensities) during burn 55, with white spruce smoke (Fig. 2). Toluene (C_7H_8) was chosen as a VOC proxy because it has a high signal-to-noise ratio, few if any interferences in PIT-MS measurements, minimal wall loss, no expected production, and a reaction rate with OH fast enough that significant toluene is removed but slow enough so that some remains to be measured by the PIT-MS. Benzene (C_6H_6) was also chosen as a VOC proxy for similar surface loss and production considerations, and has an OH reaction rate similar to SO_2, which was used in the offline calibrations. During PIT-MS measurements of the reactor output, toluene and benzene decreased

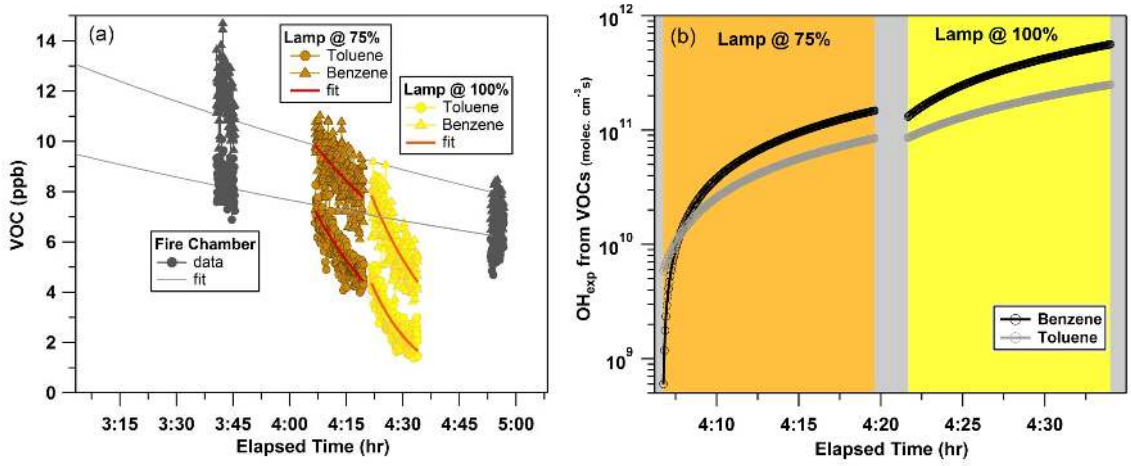

Fig. 2. Time series of VOC observations in the reactor at two different UV lamp settings used to calibrate OH_{exp}. Percentage of light reported is one lamp at 75 or 100 % of maximum supplied voltage. **(a)** Data from burn 55, white spruce, showing fire chamber measurements of toluene and benzene made by PIT-MS (gray points). A fit of the dilution of the fire chamber concentrations is shown as a solid gray line. Flow reactor measurements of toluene and benzene are colored brown and yellow, respectively. Fits of the VOC concentrations after the flow reactor were used to calculate OH concentrations. **(b)** OH_{exp} in the reactor calculated from PIT-MS benzene and toluene measurements.

not only because of reactions with OH but also because of dilution of the smoke. Separating these two concurrent decays required the fire chamber dilution of VOCs to be determined by fitting an exponential decay curve to VOC concentrations drawn directly from the fire chamber (Fig. 2a). Assuming the additional decay was due only to reaction with OH, the concentration of OH can be estimated from Eq. (2).

$$[\mathrm{VOC}]_{\mathrm{out}} = [\mathrm{VOC}]_0 e^{-(k[\mathrm{OH}]\Delta \mathrm{t})}, \quad (2)$$

where $[\mathrm{VOC}]_0$ is the mixing ratio of the VOC (toluene or benzene) entering the reactor, and $[\mathrm{VOC}]_{\mathrm{out}}$ is the mixing ratio exiting the reactor. For toluene, $k_{\mathrm{OH}} = 5.63 \times 10^{-12}\,\mathrm{cm^3\,molecule^{-1}\,s^{-1}}$, and for benzene $k_{\mathrm{OH}} = 1.22 \times 10^{-12}\,\mathrm{cm^3\,molecule^{-1}\,s^{-1}}$ (Atkinson and Arey, 2003). Δt is the residence time in the flow reactor (180 s). The results of calculating the OH concentration in the reactor for burn 55 are shown in Fig. 2b. With one lamp at 75 % of its max voltage, OH_{exp} is estimated at 1.5×10^{11} and 8.5×10^{10} molecules $\mathrm{cm^{-3}}$ s using benzene and toluene, respectively. With one lamp at 100 %, OH_{exp} is estimated at 5.6×10^{11} and 2.5×10^{11} molecules $\mathrm{cm^{-3}}$ s using benzene and toluene, respectively.

The OH_{exp} calibration equation (Eq. 1) was adjusted to account for OH suppression by comparing the OH_{exp} calculated by offline SO_2 calibration and OH_{exp} from real-time VOC decays (Fig. S6). The difference between these OH estimation methods using online benzene and toluene measurements was combined to obtain an average suppression factor of 3.7 ± 0.28 (average $\pm 1\sigma$); that is, OH was an average of 3.7 times lower than calculated using the offline SO_2 calibration. This factor was applied to Eq. (1), and is used for all experiments where OH_{exp} is presented. Taking OH suppression into account, OH_{exp} in this study ranged from 1.36×10^{10} to 6.5×10^{11} molec. $\mathrm{cm^{-3}}$ s, equivalent to 0.1–5.0 days of photochemical aging. Due to the high OH reactivity of our samples (estimated to be $15\,500\,\mathrm{s^{-1}}$), this range of OH exposures is lower than in other experiments using a similar flow reactor configuration because of the high VOC levels.

3 Results

3.1 Observations

Following each biomass fuel's ignition, aerosol and VOC concentrations increased rapidly during the first 10 min as smoke mixed throughout the chamber. Peak concentrations were observed within 15 min from fire ignition. Maximum concentrations were followed by a slow decay over a few hours because of FSL fire chamber dilution with ambient air of much lower aerosol concentrations. Over the course of a typical 3.5 h measurement period, unprocessed smoke drawn from the fire chamber slowly diluted on average by a factor of 4.5 ± 2.2 (mean from all experiments $\pm 1\sigma$) as measured from peak OA at the start of the burn.

3.1.1 VOC observations

Comparing VOC concentrations from the flow reactor in the absence of photochemical aging ($OH_{exp} = 0$) and air drawn directly from the fire chamber through tubing that bypassed the reactor showed no significant mass spectral differences when scaled for ongoing fire chamber dilution. Hence, the flow reactor itself does not appear to affect either the concentration or the composition of the VOC mixture measured

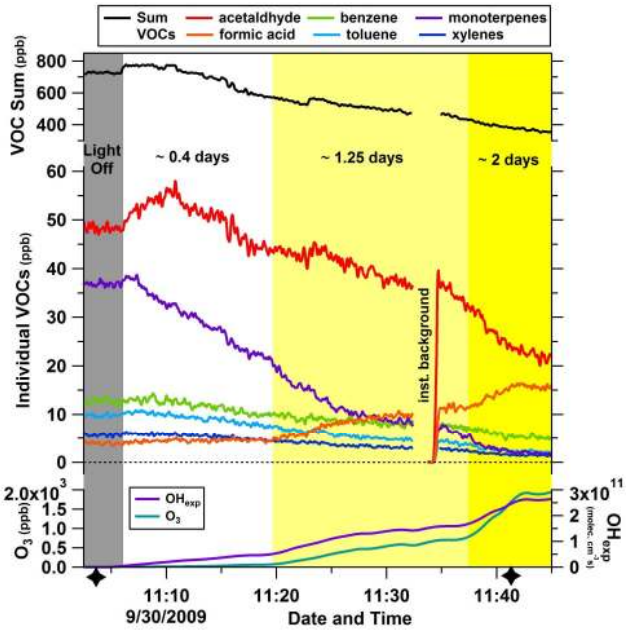

Fig. 3. Time series for select VOCs and oxidants measured after the reactor during burn 55, white spruce. The time series begins with lights off in the reactor, then transitions to increasing O_3 concentration (blue, bottom panel) and OH exposures (purple, bottom panel) in steps. The reactor was sampled with lights off (gray), then at $OH_{exp} = 5.2 \times 10^{10}$ molec. cm^{-3} s (~0.4 days aging, white), $OH_{exp} = 1.6 \times 10^{11}$ molec. cm^{-3} s (~1.25 days aging, light yellow), and $OH_{exp} = 2.6 \times 10^{11}$ molec. cm^{-3} s (~2 days aging, bright yellow). Diamond markers indicate where the mass spectra presented in Fig. 4 were taken.

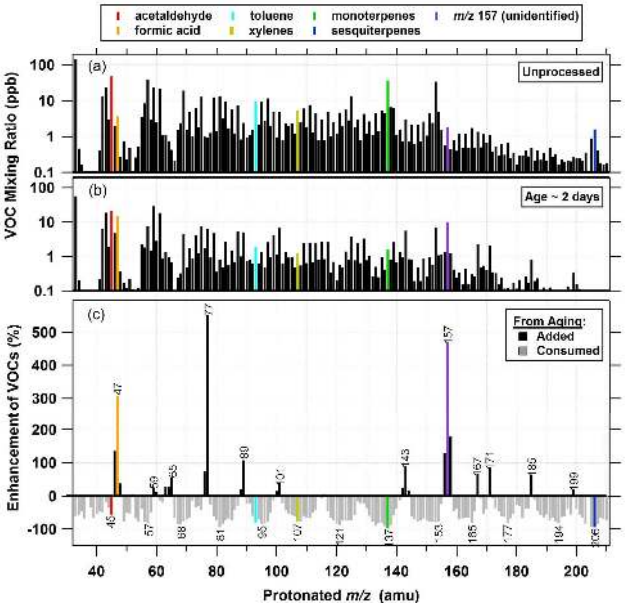

Fig. 4. PIT-MS mass spectra showing the changes in VOC composition with photochemical age, i.e., OH exposure. **(a)** Mass spectrum after the flow reactor with $OH_{exp} = 0$ (unprocessed). **(b)** Mass spectrum after the flow reactor with $OH_{exp} = 2.6 \times 10^{11}$ molec. cm^{-3} s (~2 days aging). **(c)** Percentage enhancement of VOCs in the flow reactor between unprocessed and aged. The data are from the same experiment shown in Fig. 3 (mass spectra taken at times indicated by black diamonds on the x axis Fig. 3, which shows associated OH exposures). Each spectrum is the average of 50 PIT-MS trapping cycles of 2 s. The same VOCs shown in Fig. 3 are highlighted here (with the addition of sesquiterpenes).

with the PIT-MS. VOC abundances evolved during burn experiments as the sample air was exposed to different degrees of OH exposure. Figure 3 shows the evolution of some key VOCs for wire grass (burn 56). The total measured VOCs decrease over the sample period was due to dilution. As OH exposure increased, xylenes, monoterpenes, toluene, and benzene decreased, while formic acid increased. Acetaldehyde initially increased at lowest OH exposure, and then decreased with higher exposure, suggesting that it may be an initial oxidation product before additional photochemistry degraded it. Formic acid was present in the raw smoke, and was greatly enhanced by aging. Several unidentified compounds (e.g., m/z 157, not shown in Fig. 3 for simplicity) follow the temporal trend of formic acid, indicating that they evolved from photochemical production. Similar production of formic acid and unidentified compounds (such as m/z 157) have been observed with PTR-MS measurements in chamber oxidation of terpenes (Lee et al., 2006).

PIT-MS mass spectra (Fig. 4) for the same burn as Fig. 3 illustrate the effect of photochemical aging on VOC composition. During a similar study, Warneke et al. (2011) was able to identify less than 40 % of the total PIT-MS signal in most burn experiments. Besides the trends already illustrated in Fig. 3, the full mass spectrum allows for examination of whether unidentified VOC masses increase or decrease with aging (Fig. 4c). The majority of the m/z detected decrease with aging as seen in Fig. 4c; however, about two dozen VOCs are enhanced by aging such as m/z 157, 167, and 171.

3.1.2 Aerosol observations

The continuous time series of AMS measurements show a sawtooth pattern (Fig. S2), reflecting the switching from sampling aged and unprocessed smoke. Once separated, the time series of OA in Fig. 5a shows aged and unprocessed smoke for two fuels – turkey oak (burn 45) and ponderosa pine (burn 40). For turkey oak smoke, the resultant OA mass after aging is higher than POA. In contrast, for ponderosa pine smoke, total aged OA is lower than POA after aging. Two AMS chemical markers are shown in Fig. 5. The signal at m/z 44, which is dominated by both CO_2^+ and $C_2H_4O^+$ (see Fig. S7 for details), is a marker of oxidized species, and can come from the original POA, SOA, or heterogeneous oxidation of POA. The signal at m/z 60 – which is dominated in this study by $C_2H_4O_2^+$, a fragment from levoglucosan and

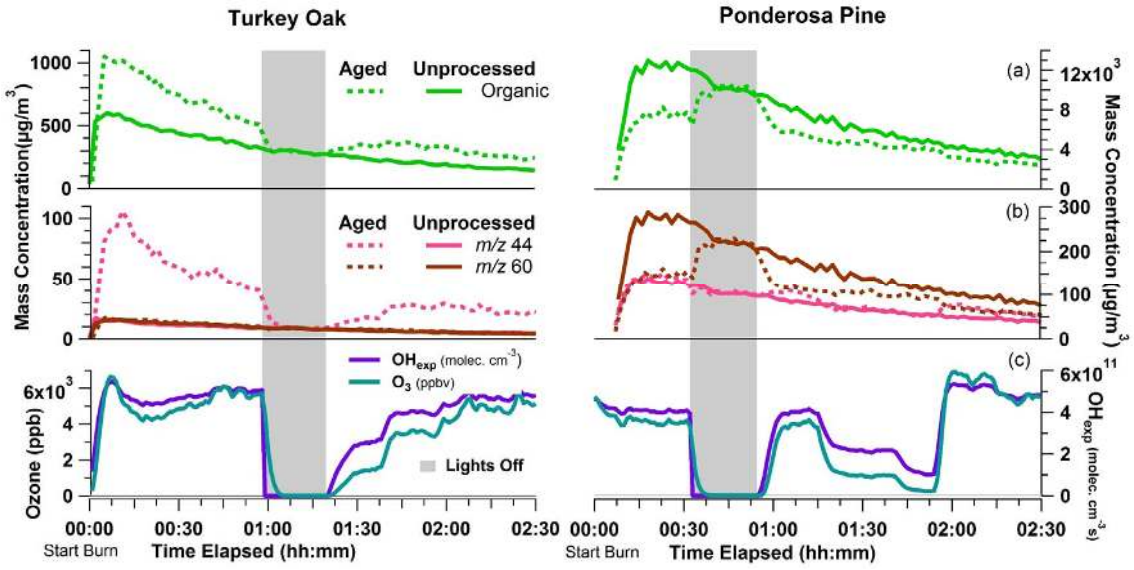

Fig. 5. Time series of OA data for turkey oak (burn 45) and ponderosa pine (burn 40) smokes. **(a)** OA mass concentration, **(b)** oxidation marker (m/z 44) and primary biomass-burning marker (m/z 60), **(c)** O_3 and OH exposure. The gray boxes denote a period when the UV lights in the flow reactor are turned off.

similar POA species – is often used as a tracer for primary biomass-burning emissions (Cubison et al., 2011; Lee et al., 2010; Ng et al., 2011b). m/z 60 can also have a contribution at $C_2H_4O_2^+$ from SOA due to species such as organic acids.

Tracers m/z 44 and m/z 60 show similar temporal trends as OA, with peak values at the start of burns and a decrease due to dilution. The oxidation tracer m/z 44 is enhanced by photochemical aging more in turkey oak smoke than in ponderosa pine smoke (Fig. 5b), and is increased with intensified aging (Fig. 5c) due to the increase of the CO_2^+ ion. The POA tracer m/z 60 is substantially depleted after aging for ponderosa pine and decreases slightly with aging, but does not change significantly for turkey oak smoke, possibly due to canceling effects from increased organic acids produced from aging or to slow diffusion in the POA that may protect levoglucosan and similar species from oxidation. The two burns presented in Fig. 5 illustrate a diverse chemical evolution upon the aging of biomass-burning smoke. The observed trends are repeatable for a given biomass, and encompass the variability of smoke aging observed over the entire campaign.

To examine potential particle losses to the walls of the reactor and tubing in the absence of aging, the reactor UV lights were turned off for 15 min after at least 30 min had passed from fuel ignition. During this "dark" period, OH exposure is negligible, and only a ~ 1 % difference in aerosol mass was observed between air that had flowed through the reactor vs. the bypass tubing, indicating minimal particle mass losses in the reactor and associated tubing.

3.2 Organic aerosol enhancement

One of the key results of this experiment is the net effect of aging on OA mass. The ratio of OA mass after aging to the OA mass before aging is defined as the net OA enhancement ratio (ER_{OA} = aged/unprocessed smoke). Since the two unprocessed 1 min data points before and after each 1 min aged point are used, there is no need to further correct for the slow ongoing dilution in the chamber. $ER_{OA} = 1$ indicates no difference between the OA mass from aged vs. unprocessed smoke, while $ER_{OA} > 1$ (or < 1) indicates mass increased (or decreased) during aging. An increase of mass can be due to SOA formation as semivolatile/nonvolatile gas-phase oxidation products partition to the aerosol and/or the heterogeneous oxidation of the primary or secondary OA because the addition of oxygen can lead to increased particle mass even if no new carbon condenses from the gas phase. A decrease in mass can either be due to heterogeneous chemistry followed by evaporation of some of the products or to gas-phase reaction of semivolatiles that leads to evaporation of particle-phase species in equilibrium with them. Our measurements cannot by themselves distinguish among these processes.

Table 1 shows ER_{OA}, calculated as the maximum deviation from unity ($ER_{OA} = 1$) due to aging and sustained over a 5 min average during each burn experiment, with associated OH_{exp} reported. ER_{OA} varies strongly with OH_{exp} and fuel type (Fig. 6). These four biomass fuels are good examples to illustrate the diversity of results observed for all fuels. As OH_{exp} increases, most fuels showed maximum absolute value of ER_{OA} (max. deviation from 1) around 3–4 days of aging, then leveled off even with increasing OH_{exp}. However,

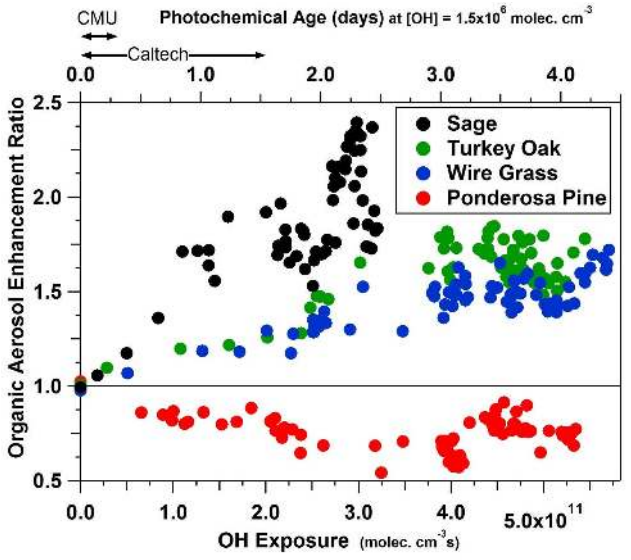

Fig. 6. OA enhancement ratio as a function of photochemical age and OH exposure for four fuels (ponderosa pine, burn 40; wire grass, burn 42; turkey oak, burn 45; and sage, burn 49). The range of OH exposure examined in smog chambers at Caltech (Chhabra et al., 2011) and Carnegie Mellon's mobile laboratory (Hennigan et al., 2011) are shown for reference.

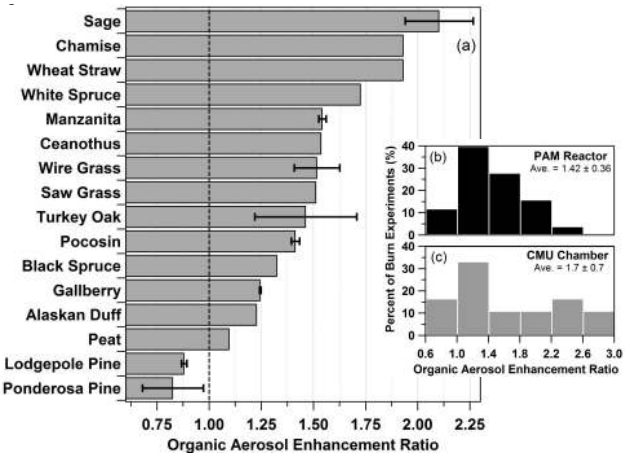

Fig. 7. Histogram of maximum 5 min averaged OA enhancement ratios for all experiments. **(a)** OA enhancement ratio of all fuels, with standard error for repeated fuels (error bars). **(b)** Histogram of organic aerosol enhancement ratio for all burns for the flow reactor and **(c)** Carnegie Mellon's mobile lab and smog chamber.

chemical transformations continued after ER_{OA} had reached a maximum deviation from unity, as discussed in more detail in Sect. 3.4. Of these four fuels, only ponderosa pine smoke showed a reduction in total OA, indicating that heterogeneous oxidation and/or evaporation of semivolatiles after aging overwhelmed any SOA formation. Sage smoke showed the highest ER_{OA}, and it is not clear whether a plateau is reached within the range of OH_{exp} achieved. This result stands in contrast to biomass-burning measurements of gas-phase emission ratios of different fuels, which show that sage smoke is similar to the smoke from other biofuels (Warneke et al., 2011). In burn 49 (sage), the organic fraction is only 70 % of the unprocessed total aerosol measured, the lowest observed. It might be expected that ER_{OA} would decrease with continuing OH_{exp} as observed in previous laboratory studies (e.g., Lambe et al., 2012), but the maximum OH_{exp} was limited in FLAME-3 by the large VOC concentrations to values below the observed turnover point for the OA mass, which was in the range of 5×10^{11}–1×10^{12} molec. cm^{-3} s.

An overview of campaign-wide maximum ER_{OA} observations shows that ER_{OA} was highly dependent on fuel type, as shown in Fig. 7a, which illustrates the maximum ER_{OA} (over a 5 min average) for all fuels, with standard error for fuels repeated in multiple burn experiments. Most ER_{OA} were reproducible within < 10 % for repeated burns of the same biomass, although a few showed more variability. The observed variability is thought to be due to variability in the burning process dynamics, which was observed visually for some fuels. This may include the fraction of the combustion time (fraction of the fuel burned) in flaming and smoldering fire phases. The burn-to-burn variability we observed was also recorded using other aging methods (Hennigan et al., 2011) within this same study, as well as in other laboratory and field biomass-burning studies (Grieshop et al., 2009; Cubison et al., 2011; Akagi et al., 2012; McMeeking et al., 2009). Aging of smoke from most fuels resulted in a net OA increase. Negligible increase or a net decrease was observed for only two fuel types: ponderosa and lodgepole pine. Figure 7b shows the statistical distribution of maximum ER_{OA} for all burns, with an average ER_{OA} of 1.42 ± 0.36 (mean $\pm 1\sigma$).

During FLAME-3, Carnegie Mellon University (CMU) deployed a mobile 7 m^3 Teflon chamber in which a combination of natural sunlight, UV blacklights, and injected nitrous acid (HONO) were the source of OH. The smoke was transferred to the chamber through a 12 m transfer line heated to 40 °C, and was diluted by a factor of ~ 25 (Hennigan et al., 2011). ER_{OA} for the CMU chamber ranged from 0.7 to 2.9, with a project average enhancement of 1.7 ± 0.7 (mean $\pm 1\sigma$). While the flow reactor sampled 25 burns during FLAME-3, CMU's chamber sampled 18. It was limited to one experiment per day because of much slower aging at lower OH exposures, and required downtime for at least 12 h of clean air flushing for bag cleaning between experiments. The distributions of maximum ER_{OA} for all burns aged in the CMU chamber are consistent with those from the flow reactor (Fig. 7c). Both aging methods observe, on average, substantial net OA enhancement from aging with a wide distribution. While CMU's data have a higher mean ER_{OA}, the median of both methods is more similar: 1.39 for the flow reactor and 1.47 for CMU's smog chamber. Smoke

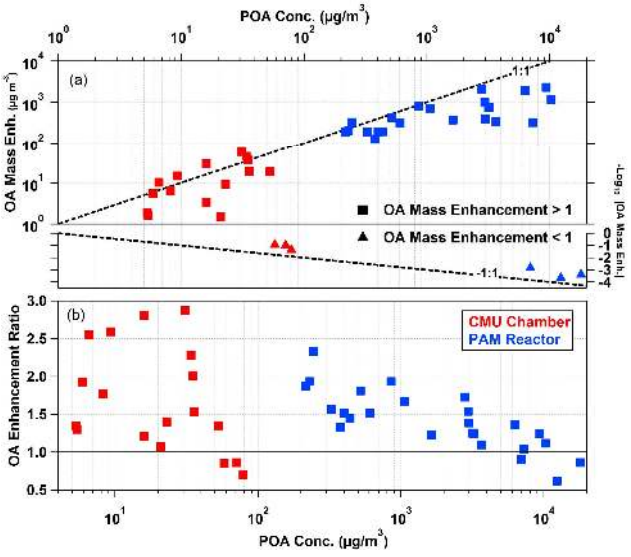

Fig. 8. OA enhancement as a function of unprocessed OA for all fuels, with CMU's mobile air-quality laboratory smog chamber (red), as reported in Hennigan et al. (2011), and flow reactor (blue). **(a)** OA mass enhancement (aged minus unprocessed) vs. POA (unprocessed). To plot data with logarithmic y axis, fuels whose aged smoke resulted in net mass loss are shown as the negative log of the absolute value of the difference between aged and unprocessed smoke, and plotted on a separate y axis. **(b)** OA enhancement ratio (i.e., relative enhancement) vs. unprocessed (POA).

from ponderosa pine burning resulted in a decrease in OA mass from both aging methods (Hennigan et al., 2011).

A possible cause for the differences between our results and CMU's are the much higher levels of dilution employed in the CMU experiment. Additional dilution decreases the gas-phase concentration of some semivolatile organics, causing net evaporation from the POA and thus reduction in OA mass (Robinson et al., 2007). During FLAME-3, smoke POA concentrations spanned two orders of magnitude. In Fig. 8a, the relationship between absolute OA mass enhancement due to aging and initial POA is shown for both our flow reactor and the CMU chamber, demonstrating that, to first order, the absolute mass enhancement due to aging scales with POA, but with a less than proportional increase at high POA values. Figure 8b shows ER_{OA} vs. initial POA for both the flow reactor and chamber. Both aging methods show a downward trend in ER_{OA} with increasing POA (with less scatter for the flow reactor data), which is qualitatively consistent with our hypothesis. Fuels whose combustion produces higher POA result in less net SOA formation when normalized to the initial POA mass. Although VOC data are only available for a few burns, the absolute or relative enhancement of OA does not correlate with the sum of the detected VOCs or with individual known precursors such as aromatics or isoprene. In addition, the total amount of SOA formed exceeds the total mass of known SOA precursors (aromatics, isoprene, monoterpenes). Both facts suggest that VOCs measured but not identified by the PIT-MS and/or that semivolatile and intermediate volatility species not measured by the PIT-MS contribute to a major fraction of the SOA formed from biomass-burning smoke. The inverse correlation of ER_{OA} with POA suggests that semivolatile and intermediate volatility species are more likely to be the dominant precursors, as more of those species will be in the gas phase at lower POA concentrations, due to gas–particle equilibrium. ER_{OA} does not appear to correlate with other burn parameters such as black carbon, NO_x, or CO emissions.

3.3 Effect of aging on chemical composition

3.3.1 Aerosol mass spectral evolution with age

To investigate chemical transformations due to smoke aging, aged vs. unprocessed AMS mass spectra are compared for two fuels, one with high ER_{OA} and one with low ER_{OA} (Fig. 9). Unprocessed spectra (Fig. 9a) show characteristics typical of biomass-burning POA spectra in the AMS, including strong signals at m/z 60 and 73 from levoglucosan and related species (Aiken et al., 2009; Lee et al., 2010). The net effect of aging on aerosol composition is calculated by subtracting the unprocessed mass spectra from those of the aged smoke (aged in Fig. 9b, difference in Fig. 9c). Aged smoke from turkey oak has an $ER_{OA} > 1$ (Fig. 6), and a few m/z decreased significantly with aging. The spectrum of the difference signal is very similar to that of fresh oxidized OA (OOA) observed in ambient air and some laboratory experiments, with similar characteristics independent of the initial POA or SOA precursor source (e.g., Jimenez et al., 2009, and references therein). Ponderosa pine has an $ER_{OA} < 1$ (Fig. 6), and most m/z, including almost all $m/z > 50$, decrease from aging, likely because of heterogeneous oxidation of the initial POA and/or evaporation of POA semivolatiles after dilution or oxidation of the gas-phase species in equilibrium with them. A few m/z increase with aging, in particular m/z 28 and 44, showing that the oxidized POA and/or SOA in this sample also evolves similarly to OOA observed elsewhere. These observations are typical of other fuels not shown, where m/z 28 and 44 always increase and spectrum-wide production or consumption tend to follow overall ER_{OA}.

The mass spectra of the ER_{OA} for these two fuels, shown in Fig. S8, exhibit similar picket-fence spacing. To summarize, we see that oxidation does not favor odd/even m/z but does have a cycle of ~ 14 m/z. These features are more distinct for ponderosa pine smoke, where mass is lost. One interpretation of the ER_{OA} mass spectral shape could be that if aging oxidizes POA without condensing new OA mass, POA should lose mass fairly equally across m/z (on a relative scale); in this case Fig. S8b would be a near flat line of ion signal < 1. However, if simultaneously adding new OA mass, with a similar spectrum to that in Fig. S8a, the combined effect could produce the ER spectrum shown

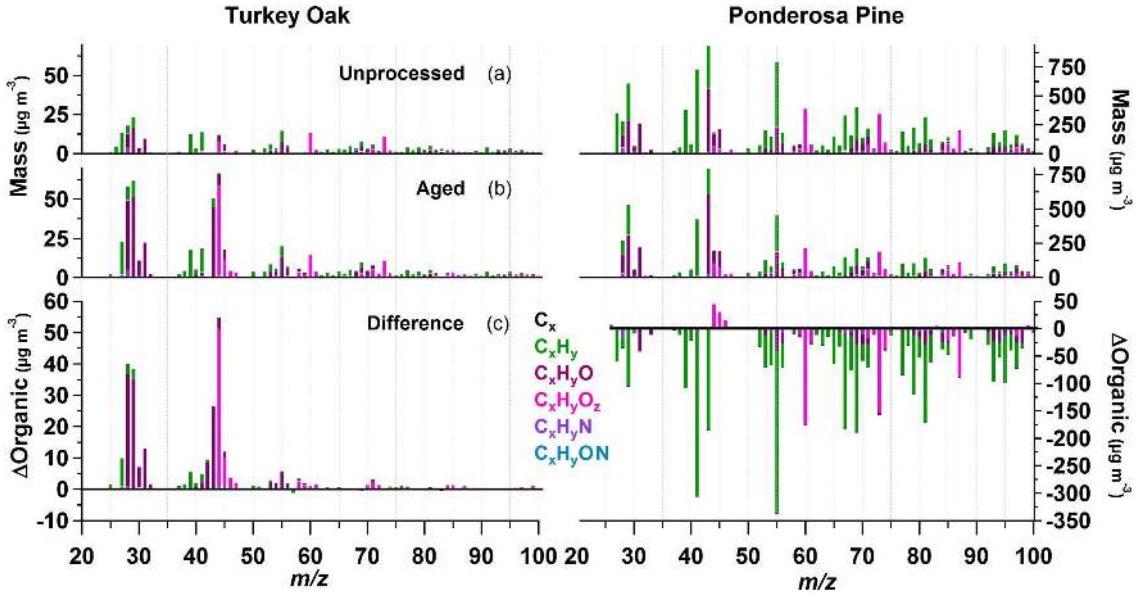

Fig. 9. Effect of photochemical processing on mass spectra of two fuels: turkey oak, burn 45, and ponderosa pine, burn 40. All data were collected 15–25 min after the start of fuel combustion and averaged over 10 min of sampling with moderate OH exposure. **(a)** Average mass spectrum of unprocessed smoke, **(b)** average mass spectrum of aged smoke, and **(c)** difference (ΔOA) between aged and unprocessed smoke. All plots are colored by ion type.

in Fig. S8b, and indeed the spectrum appears very consistent with this hypothesis. This would suggest for fuels with $ER_{OA} < 1$, aging may fragment/evaporate POA and simultaneously add new OA mass (through condensation or heterogeneous addition of oxygenated functional groups) of similar signature to other burns where ER_{OA} is > 1.

Examining chemical transformations from aging shows increased signal at m/z 28 and 44 (Fig. 9c and Fig. S8). High-resolution data show these signals are dominated by increases in CO^+ (enhanced CO^+ ion at m/z 28 in Figs. S5, S7) and CO_2^+ ions (Fig. S7), with small contributions from $C_2H_4^+$ and $C_2H_4O^+$, respectively. Note that at m/z 44, unprocessed smoke can have a higher contribution from $C_2H_4O^+$ than CO_2^+, as seen for Ponderosa Pine in Fig. S7; however, these two ions have comparable signals after aging.

3.3.2 Changes of AMS fractional tracer ion contributions (f_x) with aging

The fractional contribution of a specific m/z to total OA mass (f_x) provides information on the OA chemical transformations with aging. Previous studies have used f_{44} (m/z 44/OA) as a tracer of SOA and aging, f_{43} (m/z 43/OA) as a tracer of POA and fresh SOA, and f_{60} (m/z 60/OA) as a tracer of biomass-burning POA (Cubison et al., 2011; Ng et al., 2010). To characterize the aging of biomass-burning smoke, Cubison et al. (2011) proposed the use of the scatterplot f_{44} vs. f_{60}, which facilitated comparison of ground, aircraft, and laboratory observations. Results from Cubison et al. (2011) showed that very aged smoke can retain an elevated f_{60} signature above background levels.

The evolution of f_{44} with aging for smoke from four fuels is shown in Fig. 10a. As expected, f_{44} always increases with OH_{exp}, though to a lesser degree in experiments with fuels having an $ER_{OA} < 1$ (in part due to the decrease of ions other than CO_2^+, Fig. S7). To compare aged smoke with atmospheric measurements of OA, typical ranges of f_{44} for semivolatile oxidized organic aerosol (SV-OOA) and low-volatility oxidized organic aerosol (LV-OOA) (Jimenez et al., 2009; Ng et al., 2010) are shown on the right in Fig. 10a. The fresh smoke from turkey oak and wire grass falls at the lower end of the SV-OOA range of ambient measurements, and approaches the higher end at maximum aging. In contrast, fresh sage smoke falls well within the SV-OOA range, and reached the LV-OOA range after 1.5 days of aging. For all experiments, the rate at which f_{44} changed as the OA oxidized differs for each fuel, and this rate appears to increase with initial f_{44} of POA. We speculate that the observations in Fig. 10a are due to greater fractional partitioning of SVOCs to the particles at higher OA concentrations. Since the oxidation kinetics of SVOCs are substantially slower in the particle phase compared to the gas phase (e.g., May et al., 2012), such partitioning would result in less gas-phase oxidation and thus less of an increase in f_{44} for the fuels with higher initial POA concentrations.

A similar approach can be used to investigate the decay of f_{60} (Fig. 10b). Smoke from wire grass and turkey oak (both with $ER_{OA} > 1$) shows decreasing f_{60} with increasing aging;

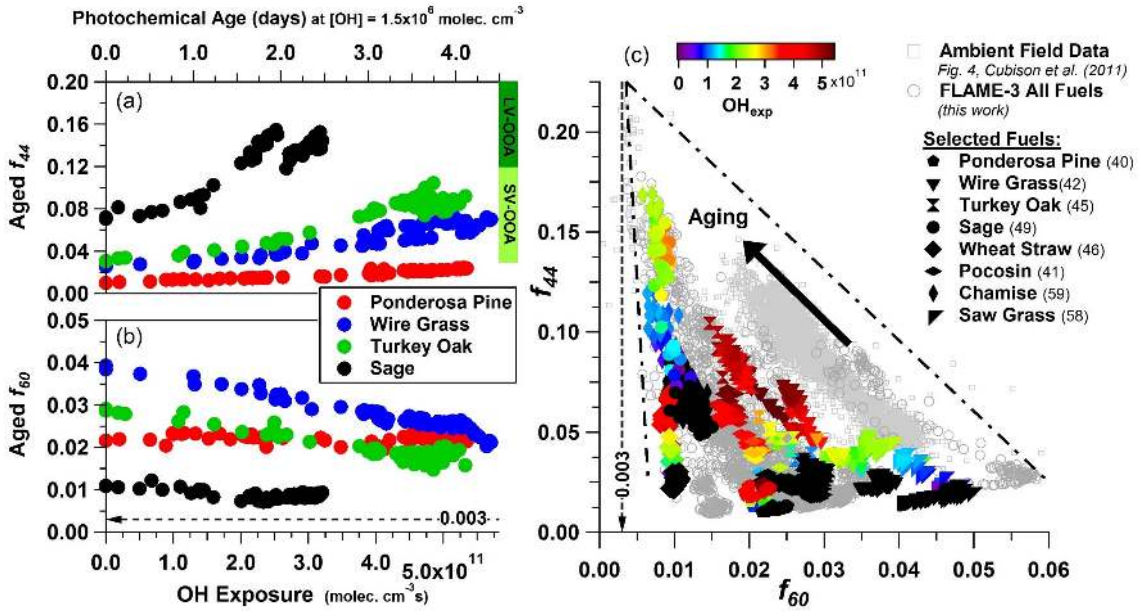

Fig. 10. Fractional contribution of oxidation and biomass-burning tracers evolution with age. **(a)** f_{44} vs. OH exposure for aged smoke from four biofuels. Light- and dark-green bars on the right respectively denote the range of values for semivolatile oxygenated-organic aerosol (SV-OOA) as defined by Ng et al. (2010) and low-volatility oxygenated-organic aerosol (LV-OOA) as defined by Aiken et al. (2009). **(b)** f_{60} vs. OH exposure for aged smoke from four biofuels. Dashed line is ambient background f_{60} level in the absence of biomass burning (Cubison et al., 2011). **(c)** Aging effects on oxidation and biomass-burning markers, f_{44} vs. f_{60}. Adapted from Cubison et al. (2011) Fig. 5, with unprocessed smoke (black markers) and aged smoke (colored by increasing OH exposure) for eight selected fuels (ponderosa pine, burn 40; wire grass, burn 42; turkey oak, burn 45; sage, burn 49; pocosin, burn 41; wheat straw, burn 46; saw grass, burn 58; and chamise, burn 59). All burns from FLAME-3 (gray circles) and field data from Fig. 4 (gray squares) of Cubison et al. (2011) are presented for reference.

in contrast, smoke from sage and ponderosa pine shows a constant f_{60} with age. Across all experiments, f_{60} always remained elevated above background ambient biomass-burning free levels ($\sim 0.3\,\% \pm 0.06\,\%$; Aiken et al., 2009; DeCarlo et al., 2008; Cubison et al., 2011). Plots of f_{60} vs. POA for unprocessed smoke (Fig. S9b) showed an increase in f_{60} at the lower POA concentrations, followed by a stabilization and then a small decrease at the highest concentrations.

While aging always increased f_{44}, it does so at very different rates for different smokes. The relationship between f_{44} and f_{60} is shown in Fig. 10c. f_{60} decreased for the majority of fuels, which can be due to gain of new SOA mass with low f_{60} and/or to reaction or volatilization of levoglucosan and similar POA species. In a few burns (where $ER_{OA} < 1$) f_{60} remained unchanged despite aging by OH, indicating that m/z 60 was reduced by aging proportionally to the rest of the OA. Regardless of decay or not, f_{60} remains elevated above background levels (in the absence of biomass burning) for all fuels (Fig. 10c). As the CO_2^+ ion is the main oxidation reaction product at m/z 44, the relation between $f_{CO_2}{}^+$ and f_{60} (Fig. S9c) is very similar to that of f_{44} and f_{60}, though the rise is $f_{CO_2}{}^+$ is sharper with increased aging.

These results are consistent with those observed in the field by Cubison et al. (2011), forming and filling a triangle of f_{44} vs. f_{60} space for aging of biomass-burning smoke. POA measured in this study have f_{60} values consistent with ambient fire plumes (Cubison et al., 2011), while f_{60} values from traditional chamber-smoke aging experiments (Hennigan et al., 2011) are much lower than ambient measurements in smoke plumes. Huffman et al. (2009) showed using a thermal denuder that m/z 60 had consistently higher volatility than the bulk OA for smoke from burning multiple biomasses, which is consistent with our data vs. POA concentration discussed above. Thus, the difference in f_{60} between the different aging methods is due to high dilution of fresh smoke into a chamber that may result in higher fractional evaporation of the species producing m/z 60.

A different triangle plot of f_{44} vs. f_{43} has been used to study aging of OOA and other OA types, where OOA ambient observations across many field studies, described by Ng et al. (2010), lie within lines forming a triangle. Multiple field and laboratory studies observed that during early stages of aging, f_{43} increases (Ng et al., 2011a). In contrast, for ongoing aging, f_{44} increases as f_{43} decreases. High-resolution AMS measurements from previous studies have shown that this shift is due to increased CO_2^+ with aging, which results in increased f_{44}, while further oxidation of molecules that produce $C_3H_7^+$ and $C_2H_3O^+$ in the AMS at m/z 43 reduces these signals with aging (Aiken et al., 2008; DeCarlo et al., 2010). Figure 11a shows f_{44} plotted vs. f_{43} from the aging

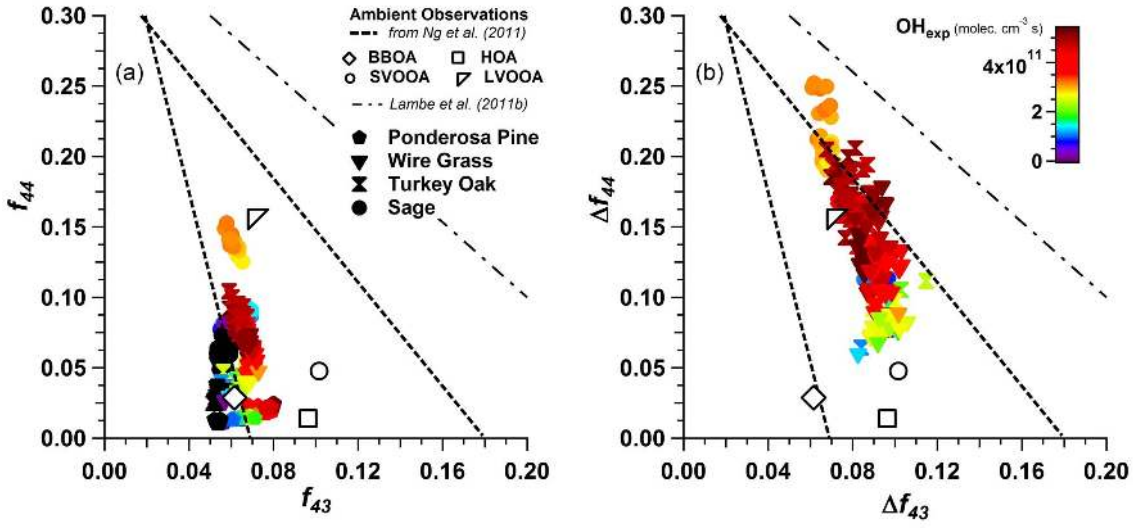

Fig. 11. Aging effect on oxidation and SOA markers. **(a)** f_{44} vs. f_{43} from four fuels. The window of observed ambient OOA is within the black dotted lines (Ng et al., 2010), and the window of the flow-reactor-observed values is within the dash-dotted lines (Lambe et al., 2011b). **(b)** Change in f_{44} and f_{43} due only to added SOA mass, where Δf_{44} is plotted with respect to Δf_{43}. In both plots, all fuels are colored by OH exposure with maximum at 5.38×10^{11} molecules cm^{-3} s. Ambient multistudy average BBOA, HOA, SVOOA, and LVOOA factors are shown for reference from Ng et al. (2011b).

of smoke from four biomasses. POA from fuels are located towards the lower-left corner, consistent with ambient observations of primary BBOA, and exemplified by average factors determined from positive matrix factorization of multiple studies from Ng et al. (2011b). With increased OH_{exp}, all fuels, at first, show a trajectory upward and to the right, moving into the window of atmospheric SV-OOA. With increasing aging, the trajectory begins to turn as f_{44} begins to increase, and f_{43} remains constant or decreases. This change is true for all burns in which ER_{OA} is > 1. f_{43} continually increases with aging for ponderosa pine smoke (and other fuels with ER_{OA} < 1). These patterns are very consistent with those reported for other photooxidation flow tubes and chamber studies presented in Ng et al. (2010) for oxidation of hydrocarbon-like OA (HOA), POA, and biogenic precursors.

The presence of high initial POA concentrations in these experiments complicates the comparison against the OOA-only evolution discussed by Ng et al. (2010). To examine the evolution of f_{44} and f_{43} due to SOA formation only, the f_{44} of only the added mass (Δf_{44}) is plotted with respect to the f_{43} of only the added mass (Δf_{43}) in Fig. 11b. Δf_x is calculated by Eq. (3),

$$\Delta f_X = \frac{\Delta C_X}{\Delta C_{OA}} = \frac{C_X(\text{Aged}) - C_X(\text{Unprocessed})}{C_{OA}(\text{Aged}) - C_{OA}(\text{Unprocessed})}, \quad (3)$$

where C_X is the concentration at m/z X and C_{OA} is the organic mass from either aged or unprocessed smoke. This parameterization assumes the POA remains unchanged, and it is only meaningful for fuels with ER_{OA} > 1. Using this metric, relatively high f_{44} in the added SOA is observed, starting near typical ambient SV-OOA and then surpassing ambient LV-OOA levels (Fig. 11b). This trend is seen in other laboratory applications of the flow reactor, where aging rapidly increases f_{44} beyond the right boundary of the triangle of ambient observations (Lambe et al., 2011b). Thus, the qualitative chemical evolution of biomass-burning OA and SOA with aging is similar to that observed for OA and SOA from other sources, consistent with previous studies (e.g., Jimenez et al., 2009).

3.4 Effect of aging on elemental composition

The high-resolution capability of the AMS allows for quantification of OA elemental composition. For all experiments, the campaign average POA O / C was 0.30 ± 0.07 and spanned the range of 0.15–0.5, while OA after aging (SOA and OPOA) had a campaign average O / C of 0.43 ± 0.14, with a maximum of 0.87.

Figure 12a shows O / C as a function of OH_{exp} for four fuels. Lambe et al. (2012) used this type of plot to assess the correlation of O / C with OH_{exp} for reactor-generated SOA from alkane precursors (gray-shaded area). All burns present in Fig. 12a are in or near that range and evolve similarly as for alkane precursor SOA, except for sage, where initial O / C is higher and increases faster with OH_{exp} (similar to f_{44} in Fig. 10). The differences between the O / C at zero OH_{exp} for these four cases show the varying degree of oxidation of fresh smoke POA. The corresponding increases of O / C with the increase of oxidation suggest that the degree of oxidation of initial POA affects the rate of increase and maximum O / C from aging.

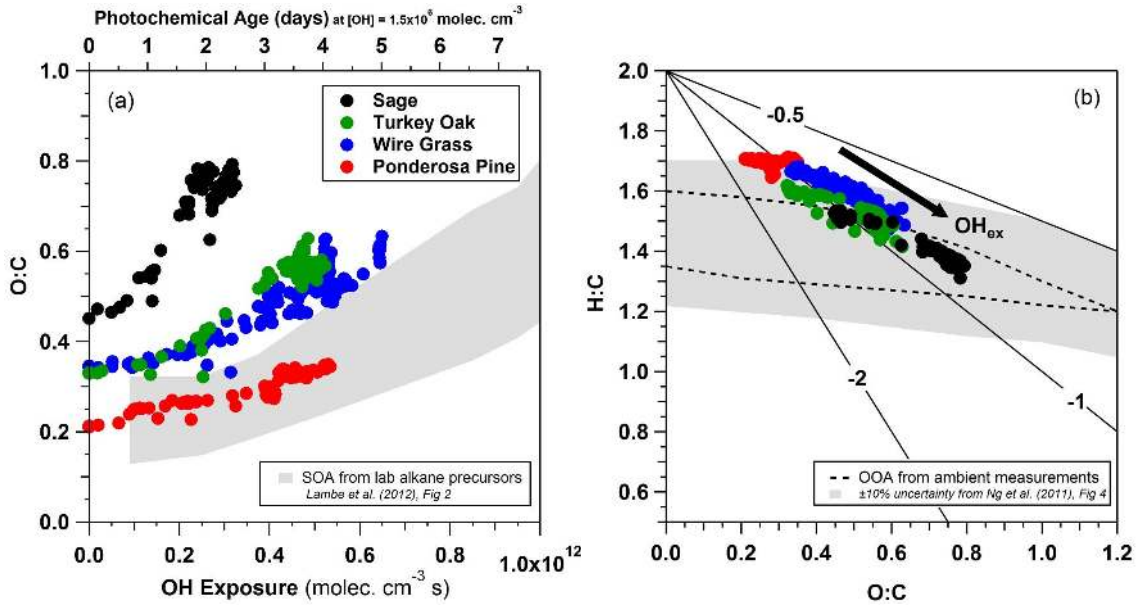

Fig. 12. Effect of smoke aging on OA elemental composition. **(a)** Oxygen-to-carbon (O / C) ratio of aged smoked as a function of OH exposure for four fuels. Results from laboratory experiments using a flow reactor to investigate SOA from alkane precursors are shown in gray from Lambe et al. (2012). **(b)** Van Krevelen diagram, showing H / C vs. O / C for four fuels. Solid lines are slopes from Heald et al. (2010), dashed lines are ambient measurements of OOA data first presented in f_{44}/f_{43} space in Ng et al. (2010), and are transformed into Van Krevelen space in the work of Ng et al. (2011) with shaded region denoting $\pm 10\,\%$ uncertainty.

Elemental ratios provide insight into oxidation mechanisms because different types of functionalization and fragmentation result in different relative evolutions in H / C and O / C ratios (Van Krevelen, 1950). Figure 12b shows the evolution of OA as H / C vs. O / C with aging from the same four burns. As OH_{exp} increases, O / C increases and H / C decreases, but at a slower rate than O / C increases. Slopes corresponding to different functionalization pathways are shown in Fig. 12b for reference. Each fuel has a unique slope, suggesting different oxidation functionalization for each fuel, as highlighted for these six fuels in Fig. S10a. Ponderosa pine, burn 40, has a slope of 0.02 ± 0.03, suggesting alcohol/peroxide functionalization (although the range was small for that burn), while the other fuels have a slope close to -0.5. Together, the range of elemental ratios from all fuels, as seen in Fig. S10b, have a trajectory that falls between the slopes lines of -1 and -0.5, consistent with the addition of both acid and alcohol functional groups without fragmentation or the addition of acid groups with carbon–carbon bond breakage. Aged smoke from this study falls within the window of ambient measurements (Ng et al., 2011a).

The relationship between O / C and f_{44} can be useful since many AMS instruments can only produce unit-resolution data, as well as for quick-look analysis of high-resolution data during data acquisition. Examining the relationship of O / C and f_{44} (Fig. 13), aged and unprocessed smoke from different fuels follow relatively similar slopes, with the exception of ponderosa pine. Using ambient ground and aircraft

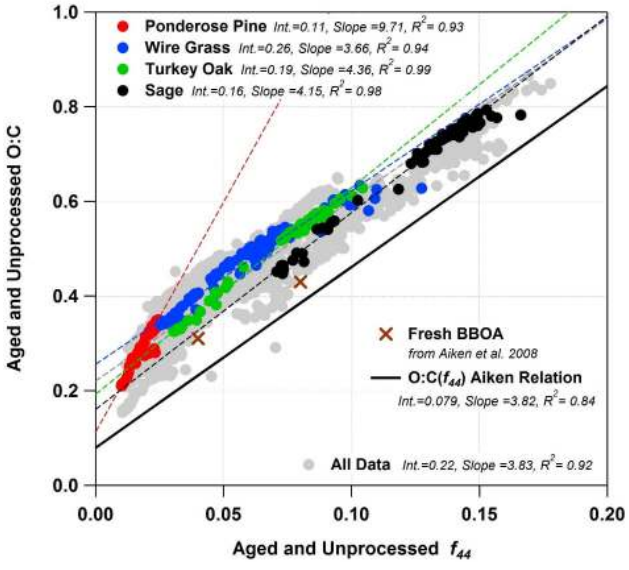

Fig. 13. Aged and unprocessed smoke O / C as a function of f_{44} for all burns with four fuels highlighted (ponderosa pine, burn 40; wire grass, burn 42; turkey oak, burn 45; and sage, burn 49). Each highlighted burn, as well as all data, is fitted with a linear ODR fit. The fit of Aiken et al. (2008) of O / C vs. f_{44} for ambient Mexico City measurements is plotted with BBOA-only data from that study highlighted for reference.

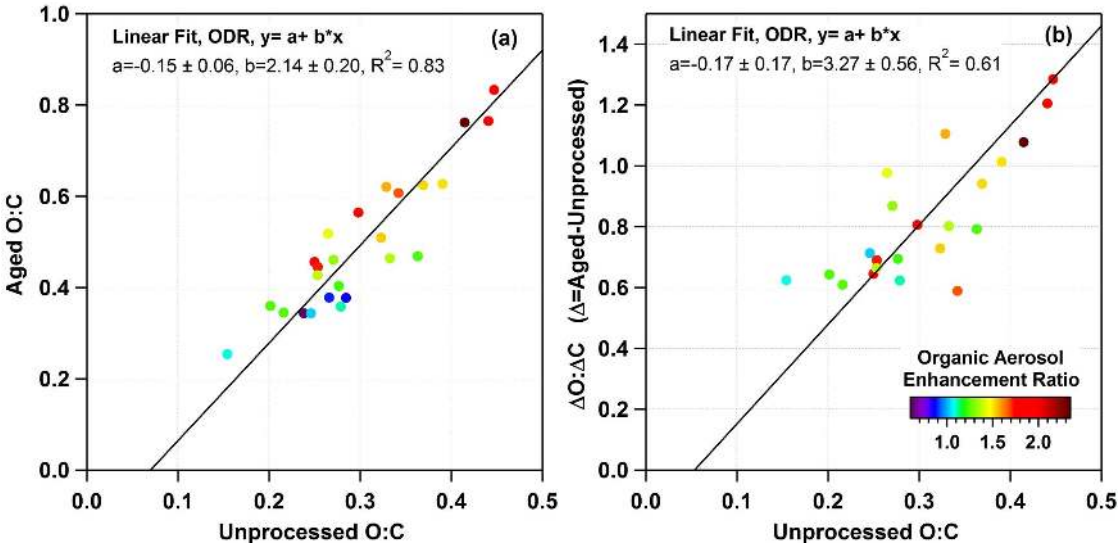

Fig. 14. Changes in O / C from aging fresh smoke. **(a)** Maximum O / C from aging as a function of unprocessed smoke O / C. **(b)** The ratio of change in oxygen (aged/unprocessed) to the change in carbon (aged/unprocessed) as a function of unprocessed O / C for fuels where this ratio is positive ($ER_{OA} > 1$). Both plots are colored by organic aerosol enhancement ratio (ER_{OA}).

AMS measurements near Mexico City, Aiken et al. (2008) reported an O / C vs. f_{44} slope of 3.82, while the slope of all burns in this study is 3.83. Although the lines are nearly parallel, there is a vertical offset for smoke data that results in higher O / C for the same f_{44} compared to the ambient data. Additionally, BBOA-only data from the field measurements of Aiken et al. (2008) are plotted in Fig. 13, and show a similar offset to the data from this study. Thus, it seems for both biomass-burning POA and SOA, f_{44} is a reasonable surrogate for O / C if high-resolution data are not available, but the difference in the offsets should be kept in mind.

Using maximum O / C after aging from each burn experiment and the corresponding O / C of POA (unprocessed) during each burn experiment, Fig. 14a shows that maximum O / C after aging is strongly correlated with O / C of unprocessed OA. Figure 14b shows the O / C of the net mass added (under the assumption that POA remains constant). The ratio of net change in oxygen to the net change in carbon from aging, i.e., the O / C of the added SOA (equivalent to Eq. 3), is correlated with POA O / C, showing that for each additional unit of initial O / C, the maximum O / C of the added SOA increased by 3.27 units. Since the intercept is near zero, the max O / C of the added SOA is approximately 3.27 times the O / C of the unprocessed POA. The O / C ratios of the added SOA are within the range of 0.4–1.0, reaching levels of very oxidized aerosol (produced by condensing highly oxidized SVOC and/or adding oxygen to POA). Note that calculation of net O / C mass added assumes unchanged POA, and thus results in an upper limit for the O / C of the added SOA, where $ER_{OA} < 1$ fuels are not plotted (since it would not be meaningful). Colored according to the ER_{OA} values, both plots in Fig. 14 show fuels with highest POA O / C have the highest O / C added from aging.

4 Summary and conclusions

Several experimental innovations were demonstrated in this study, which is the first real-time flow reactor aging experiment of a complex mixture, such as smoke, with real-time scanning of OH, an open-flow-through configuration, and multiplexing AMS and PIT-MS to allow for concurrent measurements of unprocessed and aged smoke. Fast photochemistry, short residence time, and controllable OH concentrations allowed for multiple burn experiments per day and scanning a large range of OH_{exp} during each experiment, thus allowing for investigation of OA enhancement and chemical evolution as a function of age for a range of biomass types.

VOC mass spectral evolution results showed aromatics and terpenes decrease with increasing OH_{exp}, while formic acid and other unidentified compounds increase. Although VOC total signal decreased with OH_{exp}, some gas-phase oxidation products increased with aging. Further exploration of gas-phase SOA precursors and products from this study and future experiments is important for identifying these compounds and understanding mechanisms governing photochemical processing.

Aging of smoke in the reactor resulted in a wide range of OA mass enhancement, 0.6–2.3, spanning from net OA mass loss to substantial SOA production. On average, considerable SOA was produced from smoke aging, with an average enhancement factor of 1.42 ± 0.36. The variability in OA enhancement observed in this study is consistent with the

literature from both field and laboratory studies of biomass-burning aging. OA mass losses are plausibly from heterogeneous oxidation and volatilization (Molina et al., 2004) or oxidation of gas-phase semivolatiles leading to fragmentation and evaporation of particle-phase species that were in equilibrium with the aerosol phase (Lambe et al., 2012; Donahue et al., 2012). The results indicate that fuels with higher POA emissions result in less relative OA enhancement from photochemical aging. This study confirms that the net-SOA-to-POA ratio of biomass-burning emissions is far lower than that observed for urban emissions (DeCarlo et al., 2010; Hayes et al., 2013). This is thought to be due to the much higher ratio of total observed organic compounds to CO found in urban emissions (Heald et al., 2008). Note that the ratio of net SOA to CO (often used to monitor the evolution of SOA in the field) is similar between both sources and can often be higher for biomass-burning emissions (Cubison et al., 2011; Jolleys et al., 2012).

As OH_{exp} was increased, most fuels showed maximum ER_{OA} (deviation from 1) around three days of photochemical age ($OH_{exp} \sim 3.9 \times 10^{11}$ molecules cm^{-3} s), then leveling off and remaining constant even with increasing OH_{exp}. Since the VOCs measured with the PIT-MS do not correlate with the enhancement of OA, the formation of net SOA suggests the importance of primary intermediate volatility and semivolatile gases as SOA precursors. Calculations suggest that while heterogeneous processes can be important in conditions where gas-phase oxidation cannot occur, that gas-phase oxidation will be more effective most of the time (Donahue et al., 2012).

Independent of net OA mass increase or decrease, some consistent chemical transformations were observed from aging in every burn experiment. m/z 28 and 44 are always enhanced (CO^+ and CO_2^+ increase), even in fuels that undergo a net mass decrease from aging ($ER_{OA} < 1$). The rate at which f_{44} changes (as the smoke from each of the fuels is oxidized) differs for each fuel, and this rate appears to increase with initial f_{44} of POA. f_{60} either remains constant or significantly decreases with increased OH_{exp} (always remaining elevated above 0.3 %, background ambient biomass-burning-free levels).

For all experiments, POA O / C spanned 0.15–0.5, with aged OA O / C ratios enhanced up to 0.87, and the O / C of added mass (when there was net enhancement) ranged from 0.4 to 1.0. The relationship of O / C with OH_{exp} for most aged smoke shows a similar increasing slope to alkane precursor SOA (Lambe et al., 2012). ER_{OA} and maximum O / C from aging correlates with the degree of oxidation of POA; therefore, POA characteristics, both intrinsic (i.e., chemical composition) and extrinsic (i.e., correlation with POA concentration), appear to be important predictors of SOA formation from biomass-burning smoke. As OH_{exp} increases, H / C vs. O / C showed different slopes for different fuels, suggesting slightly different functionalization for each biomass. The net SOA added in this study falls within the ambient OOA window of Van Krevelen space (Ng et al., 2011a).

This study shows that photochemical aging of smoke from biomass burning can account for a significant enhancement of initial emitted OA mass. These secondary processes, which include functionalization and fragmentation reactions, need to be included in climate- and air-quality models to improve our constraints on aerosol in climate and global OA budgets, as well as to support air-quality policy, forecasting, and mitigation in regions susceptible to wildfires or controlled burning.

Supplementary material related to this article is available online at http://www.atmos-chem-phys.net/13/11551/2013/acp-13-11551-2013-supplement.pdf.

Acknowledgements. We thank the DOE (BER, ASP Program DE-SC0006035) and the EPA (STAR grant R833747) for funding. A. M. Ortega acknowledges a graduate fellowship from the DOE SCGP Fellowship Program (ORAU, ORISE). W. H. Brune acknowledges the support by NSF (grant ATM-0919079). We are grateful to J. Gilman, C. Warneke, A. P. Sullivan, and G. R. McMeekin for useful discussions. We thank S. Kreidenweis of CSU for organization of the FLAME-3 experiment; C. Wold, E. Lincoln, and W. M. Hao for use of the Missoula Fire Sciences Laboratory facilities; C. Hennigan and A. Robinson for CMU collaborations; and T. Onasch for CO_2 data.

Edited by: M. C. Facchini

References

Aiken, A. C., DeCarlo, P. F., and Jimenez, J. L.: Elemental Analysis of Organic Species with Electron Ionization High-Resolution Mass Spectrometry, Anal. Chem., 79, 8350–8358, doi:10.1021/ac071150w, 2007.

Aiken, A. C., DeCarlo, P. F., Kroll, J. H., Worsnop, D. R., Huffman, J. A., Docherty, K. S., Ulbrich, I. M., Mohr, C., Kimmel, J. R., Sueper, D., Sun, Y., Zhang, Q., Trimborn, A., Northway, M., Ziemann, P. J., Canagaratna, M. R., Onasch, T. B., Alfarra, M. R., Prevot, A. S. H., Dommen, J., Duplissy, J., Metzger, A., Baltensperger, U., and Jimenez, J. L.: O / C and OM/OC Ratios of Primary, Secondary, and Ambient Organic Aerosols with High-Resolution Time-of-Flight Aerosol Mass Spectrometry, Environ. Sci. Technol., 42, 4478–4485, doi:10.1021/es703009q, 2008.

Aiken, A. C., Salcedo, D., Cubison, M. J., Huffman, J. A., DeCarlo, P. F., Ulbrich, I. M., Docherty, K. S., Sueper, D., Kimmel, J. R., Worsnop, D. R., Trimborn, A., Northway, M., Stone, E. A., Schauer, J. J., Volkamer, R. M., Fortner, E., de Foy, B., Wang, J., Laskin, A., Shutthanandan, V., Zheng, J., Zhang, R., Gaffney, J., Marley, N. A., Paredes-Miranda, G., Arnott, W. P., Molina, L. T., Sosa, G., and Jimenez, J. L.: Mexico City aerosol analysis during MILAGRO using high resolution aerosol mass spectrometry at the urban supersite (T0) – Part 1: Fine particle composi-

tion and organic source apportionment, Atmos. Chem. Phys., 9, 6633–6653, doi:10.5194/acp-9-6633-2009, 2009.

Akagi, S. K., Craven, J. S., Taylor, J. W., McMeeking, G. R., Yokelson, R. J., Burling, I. R., Urbanski, S. P., Wold, C. E., Seinfeld, J. H., Coe, H., Alvarado, M. J., and Weise, D. R.: Evolution of trace gases and particles emitted by a chaparral fire in California, Atmos. Chem. Phys., 12, 1397–1421, doi:10.5194/acp-12-1397-2012, 2012.

Alfarra, M. R., Prevot, A. S. H., Szidat, S., Sandradewi, J., Weimer, S., Lanz, V. A., Schreiber, D., Mohr, M., and Baltensperger, U.: Identification of the Mass Spectral Signature of Organic Aerosols from Wood Burning Emissions, Environ. Sci. Technol., 41, 5770–5777, doi:10.1021/es062289b, 2007.

Allan, J. D., Jimenez, J. L., Williams, P. I., Alfarra, M. R., Bower, K. N., Jayne, J. T., Coe, H., and Worsnop, D. R.: Quantitative sampling using an Aerodyne aerosol mass spectrometer 1. Techniques of data interpretation and error analysis, J. Geophys. Res., 108, 4090, doi:10.1029/2002jd002358, 2003.

Allan, J. D., Delia, A. E., Coe, H., Bower, K. N., Alfarra, M. R., Jimenez, J. L., Middlebrook, A. M., Drewnick, F., Onasch, T. B., Canagaratna, M. R., Jayne, J. T., and Worsnop, D. R.: A generalised method for the extraction of chemically resolved mass spectra from Aerodyne aerosol mass spectrometer data, J. Aerosol Sci., 35, 909–922, doi:10.1016/j.jaerosci.2004.02.007, 2004.

Atkinson, R. and Arey, J.: Gas-phase tropospheric chemistry of biogenic volatile organic compounds: a review, Atmos. Environ., 37, Supplement 2, 197–219, doi:10.1016/s1352-2310(03)00391-1, 2003.

Bahreini, R., Middlebrook, A. M., Brock, C. A., de Gouw, J. A., McKeen, S. A., Williams, L. R., Daumit, K. E., Lambe, A. T., Massoli, P., Canagaratna, M. R., Ahmadov, R., Carrasquillo, A. J., Cross, E. S., Ervens, B., Holloway, J. S., Hunter, J. F., Onasch, T. B., Pollack, I. B., Roberts, J. M., Ryerson, T. B., Warneke, C., Davidovits, P., Worsnop, D. R., and Kroll, J. H.: Mass Spectral Analysis of Organic Aerosol Formed Downwind of the Deepwater Horizon Oil Spill: Field Studies and Laboratory Confirmations, Environ. Sci. Technol., 46, 8025–8034, doi:10.1021/es301691k, 2012.

Canagaratna, M. R., Jayne, J. T., Jimenez, J. L., Allan, J. D., Alfarra, M. R., Zhang, Q., Onasch, T. B., Drewnick, F., Coe, H., Middlebrook, A., Delia, A., Williams, L. R., Trimborn, A. M., Northway, M. J., DeCarlo, P. F., Kolb, C. E., Davidovits, P., and Worsnop, D. R.: Chemical and microphysical characterization of ambient aerosols with the aerodyne aerosol mass spectrometer, Mass Spectrom. Rev., 26, 185–222, doi:10.1002/mas.20115, 2007.

Capes, G., Johnson, B., McFiggans, G., Williams, P. I., Haywood, J., and Coe, H.: Aging of biomass burning aerosols over West Africa: Aircraft measurements of chemical composition, microphysical properties, and emission ratios, J. Geophys. Res., 113, D00C15, doi:10.1029/2008jd009845, 2008.

Chhabra, P. S., Ng, N. L., Canagaratna, M. R., Corrigan, A. L., Russell, L. M., Worsnop, D. R., Flagan, R. C., and Seinfeld, J. H.: Elemental composition and oxidation of chamber organic aerosol, Atmos. Chem. Phys., 11, 8827–8845, doi:10.5194/acp-11-8827-2011, 2011.

Christian, T. J., Kleiss, B., Yokelson, R. J., Holzinger, R., Crutzen, P. J., Hao, W. M., Saharjo, B. H., and Ward, D. E.: Comprehensive laboratory measurements of biomass-burning emissions: 1. Emissions from Indonesian, African, and other fuels, J. Geophys. Res., 108, 4719, doi:10.1029/2003jd003704, 2003.

Cocker, D. R., Flagan, R. C., and Seinfeld, J. H.: State-of-the-Art Chamber Facility for Studying Atmospheric Aerosol Chemistry, Environ. Sci. Technol., 35, 2594–2601, doi:10.1021/es0019169, 2001.

Cubison, M. J., Ortega, A. M., Hayes, P. L., Farmer, D. K., Day, D., Lechner, M. J., Brune, W. H., Apel, E., Diskin, G. S., Fisher, J. A., Fuelberg, H. E., Hecobian, A., Knapp, D. J., Mikoviny, T., Riemer, D., Sachse, G. W., Sessions, W., Weber, R. J., Weinheimer, A. J., Wisthaler, A., and Jimenez, J. L.: Effects of aging on organic aerosol from open biomass burning smoke in aircraft and laboratory studies, Atmos. Chem. Phys., 11, 12049–12064, doi:10.5194/acp-11-12049-2011, 2011.

de Gouw, J. and Warneke, C.: Measurements of volatile organic compounds in the earths atmosphere using proton-transfer-reaction mass spectrometry, Mass Spectrom. Rev., 26, 223–257, doi:10.1002/mas.20119, 2007.

de Gouw, J. and Jimenez, J. L.: Organic Aerosols in the Earth's Atmosphere, Environ. Sci. Technol., 43, 7614–7618, doi:10.1021/es9006004, 2009.

DeCarlo, P. F., Kimmel, J. R., Trimborn, A., Northway, M. J., Jayne, J. T., Aiken, A. C., Gonin, M., Fuhrer, K., Horvath, T., Docherty, K. S., Worsnop, D. R., and Jimenez, J. L.: Field-Deployable, High-Resolution, Time-of-Flight Aerosol Mass Spectrometer, Anal. Chem., 78, 8281–8289, doi:10.1021/ac061249n, 2006.

DeCarlo, P. F., Dunlea, E. J., Kimmel, J. R., Aiken, A. C., Sueper, D., Crounse, J., Wennberg, P. O., Emmons, L., Shinozuka, Y., Clarke, A., Zhou, J., Tomlinson, J., Collins, D. R., Knapp, D., Weinheimer, A. J., Montzka, D. D., Campos, T., and Jimenez, J. L.: Fast airborne aerosol size and chemistry measurements above Mexico City and Central Mexico during the MILAGRO campaign, Atmos. Chem. Phys., 8, 4027–4048, doi:10.5194/acp-8-4027-2008, 2008.

DeCarlo, P. F., Ulbrich, I. M., Crounse, J., de Foy, B., Dunlea, E. J., Aiken, A. C., Knapp, D., Weinheimer, A. J., Campos, T., Wennberg, P. O., and Jimenez, J. L.: Investigation of the sources and processing of organic aerosol over the Central Mexican Plateau from aircraft measurements during MILAGRO, Atmos. Chem. Phys., 10, 5257–5280, doi:10.5194/acp-10-5257-2010, 2010.

Docherty, K. S., Jaoui, M., Corse, E., Jimenez, J. L., Offenberg, J. H., Lewandowski, M., and Kleindienst, T. E.: Collection Efficiency of the Aerosol Mass Spectrometer for Chamber-Generated Secondary Organic Aerosols, Aerosol Sci. Technol., 47, 294–309, doi:10.1080/02786826.2012.752572, 2013.

Donahue, N., Robinson, A., Trump, E., Riipinen, I., and Kroll, J.: Volatility and Aging of Atmospheric Organic Aerosol, in, Topics in Current Chemistry, Springer Berlin Heidelberg, 1–47, 2012.

Drewnick, F., Hings, S. S., Curtius, J., Eerdekens, G., and Williams, J.: Measurement of fine particulate and gas-phase species during the New Year's fireworks 2005 in Mainz, Germany, Atmos. Environ., 40, 4316–4327, doi:10.1016/j.atmosenv.2006.03.040, 2006.

Farmer, D. K., Matsunaga, A., Docherty, K. S., Surratt, J. D., Seinfeld, J. H., Ziemann, P. J., and Jimenez, J. L.: Response of an aerosol mass spectrometer to organonitrates and organosulfates and implications for atmospheric chemistry, P. Natl. Acad. Sci., 107, 6670–6675, doi:10.1073/pnas.0912340107, 2010.

Forster, P., Ramaswamy, V., Artaxo, P., Berntsen, T., Betts, R., Fahey, D. W., Haywood, J., Lean, J., Lowe, D. C., Myhre, G., Nganga, J., Prinn, R., Raga, G., Schulz, M., and Van Dorland, R.: Changes in Atmospheric Constituents and in Radiative Forcing. In: Climate Change 2007: The Physical Science Basis. Contribution of Working Group I to the Fourth Assessment Report of the Intergovernmental Panel on Climate Change, in: IPCC Fourth Assessment Report, edited by: Solomon, S., Qin, D., Manning, M., Chen, Z., Marquis, M., Averyt, K. B., Tignor, M., and Miller, H. L., Cambridge University Press, Cambridge, United Kingdom and New York, NY, USA, 2007.

Grieshop, A. P., Donahue, N. M., and Robinson, A. L.: Laboratory investigation of photochemical oxidation of organic aerosol from wood fires 2: analysis of aerosol mass spectrometer data, Atmos. Chem. Phys., 9, 2227–2240, doi:10.5194/acp-9-2227-2009, 2009.

Hallquist, M., Wenger, J. C., Baltensperger, U., Rudich, Y., Simpson, D., Claeys, M., Dommen, J., Donahue, N. M., George, C., Goldstein, A. H., Hamilton, J. F., Herrmann, H., Hoffmann, T., Iinuma, Y., Jang, M., Jenkin, M. E., Jimenez, J. L., Kiendler-Scharr, A., Maenhaut, W., McFiggans, G., Mentel, Th. F., Monod, A., Prévôt, A. S. H., Seinfeld, J. H., Surratt, J. D., Szmigielski, R., and Wildt, J.: The formation, properties and impact of secondary organic aerosol: current and emerging issues, Atmos. Chem. Phys., 9, 5155–5236, doi:10.5194/acp-9-5155-2009, 2009.

Hayes, P. L., Ortega, A. M., Cubison, M. J., Froyd, K. D., Zhao, Y., Cliff, S. S., Hu, W. W., Toohey, D. W., Flynn, J. H., Lefer, B. L., Grossberg, N., Alvarez, S., Rappenglück, B., Taylor, J. W., Allan, J. D., Holloway, J. S., Gilman, J. B., Kuster, W. C., de Gouw, J. A., Massoli, P., Zhang, X., Liu, J., Weber, R. J., Corrigan, A. L., Russell, L. M., Isaacman, G., Worton, D. R., Kreisberg, N. M., Goldstein, A. H., Thalman, R., Waxman, E. M., Volkamer, R., Lin, Y. H., Surratt, J. D., Kleindienst, T. E., Offenberg, J. H., Dusanter, S., Griffith, S., Stevens, P. S., Brioude, J., Angevine, W. M., and Jimenez, J. L.: Organic aerosol composition and sources in Pasadena, California, during the 2010 CalNex campaign, J. Geophys. Res.-Atmos., 118, 9233–9257, doi:10.1002/jgrd.50530, 2013.

Heald, C. L., Goldstein, A. H., Allan, J. D., Aiken, A. C., Apel, E., Atlas, E. L., Baker, A. K., Bates, T. S., Beyersdorf, A. J., Blake, D. R., Campos, T., Coe, H., Crounse, J. D., DeCarlo, P. F., de Gouw, J. A., Dunlea, E. J., Flocke, F. M., Fried, A., Goldan, P., Griffin, R. J., Herndon, S. C., Holloway, J. S., Holzinger, R., Jimenez, J. L., Junkermann, W., Kuster, W. C., Lewis, A. C., Meinardi, S., Millet, D. B., Onasch, T., Polidori, A., Quinn, P. K., Riemer, D. D., Roberts, J. M., Salcedo, D., Sive, B., Swanson, A. L., Talbot, R., Warneke, C., Weber, R. J., Weibring, P., Wennberg, P. O., Worsnop, D. R., Wittig, A. E., Zhang, R., Zheng, J., and Zheng, W.: Total observed organic carbon (TOOC) in the atmosphere: a synthesis of North American observations, Atmos. Chem. Phys., 8, 2007–2025, doi:10.5194/acp-8-2007-2008, 2008.

Hecobian, A., Liu, Z., Hennigan, C. J., Huey, L. G., Jimenez, J. L., Cubison, M. J., Vay, S., Diskin, G. S., Sachse, G. W., Wisthaler, A., Mikoviny, T., Weinheimer, A. J., Liao, J., Knapp, D. J., Wennberg, P. O., Kürten, A., Crounse, J. D., Clair, J. St., Wang, Y., and Weber, R. J.: Comparison of chemical characteristics of 495 biomass burning plumes intercepted by the NASA DC-8 aircraft during the ARCTAS/CARB-2008 field campaign, Atmos. Chem. Phys., 11, 13325–13337, doi:10.5194/acp-11-13325-2011, 2011.

Hennigan, C. J., Miracolo, M. A., Engelhart, G. J., May, A. A., Presto, A. A., Lee, T., Sullivan, A. P., McMeeking, G. R., Coe, H., Wold, C. E., Hao, W.-M., Gilman, J. B., Kuster, W. C., de Gouw, J., Schichtel, B. A., J. L. Collett Jr., Kreidenweis, S. M., and Robinson, A. L.: Chemical and physical transformations of organic aerosol from the photo-oxidation of open biomass burning emissions in an environmental chamber, Atmos. Chem. Phys., 11, 7669–7686, doi:10.5194/acp-11-7669-2011, 2011.

Heringa, M. F., DeCarlo, P. F., Chirico, R., Tritscher, T., Dommen, J., Weingartner, E., Richter, R., Wehrle, G., Prévôt, A. S. H., and Baltensperger, U.: Investigations of primary and secondary particulate matter of different wood combustion appliances with a high-resolution time-of-flight aerosol mass spectrometer, Atmos. Chem. Phys., 11, 5945–5957, doi:10.5194/acp-11-5945-2011, 2011.

Huffman, J. A., Docherty, K. S., Mohr, C., Cubison, M. J., Ulbrich, I. M., Ziemann, P. J., Onasch, T. B., and Jimenez, J. L.: Chemically-Resolved Volatility Measurements of Organic Aerosol from Different Sources, Environ. Sci. Technol., 43, 5351–5357, doi:10.1021/es803539d, 2009.

Jimenez, J. L., Canagaratna, M. R., Donahue, N. M., Prevot, A. S. H., Zhang, Q., Kroll, J. H., DeCarlo, P. F., Allan, J. D., Coe, H., Ng, N. L., Aiken, A. C., Docherty, K. S., Ulbrich, I. M., Grieshop, A. P., Robinson, A. L., Duplissy, J., Smith, J. D., Wilson, K. R., Lanz, V. A., Hueglin, C., Sun, Y. L., Tian, J., Laaksonen, A., Raatikainen, T., Rautiainen, J., Vaattovaara, P., Ehn, M., Kulmala, M., Tomlinson, J. M., Collins, D. R., Cubison, M. J., Dunlea, E. J., Huffman, J. A., Onasch, T. B., Alfarra, M. R., Williams, P. I., Bower, K., Kondo, Y., Schneider, J., Drewnick, F., Borrmann, S., Weimer, S., Demerjian, K., Salcedo, D., Cottrell, L., Griffin, R., Takami, A., Miyoshi, T., Hatakeyama, S., Shimono, A., Sun, J. Y., Zhang, Y. M., Dzepina, K., Kimmel, J. R., Sueper, D., Jayne, J. T., Herndon, S. C., Trimborn, A. M., Williams, L. R., Wood, E. C., Middlebrook, A. M., Kolb, C. E., Baltensperger, U., and Worsnop, D. R.: Evolution of Organic Aerosols in the Atmosphere, Science, 326, 1525–1529, doi:10.1126/science.1180353, 2009.

Jolleys, M. D., Coe, H., McFiggans, G., Capes, G., Allan, J. D., Crosier, J., Williams, P. I., Allen, G., Bower, K. N., Jimenez, J. L., Russell, L. M., Grutter, M., and Baumgardner, D.: Characterizing the Aging of Biomass Burning Organic Aerosol by Use of Mixing Ratios: A Meta-analysis of Four Regions, Environ. Sci. Technol., 46, 13093–13102, doi:10.1021/es302386v, 2012.

Kang, E., Root, M. J., Toohey, D. W., and Brune, W. H.: Introducing the concept of Potential Aerosol Mass (PAM), Atmos. Chem. Phys., 7, 5727–5744, doi:10.5194/acp-7-5727-2007, 2007.

Kang, E., Toohey, D. W., and Brune, W. H.: Dependence of SOA oxidation on organic aerosol mass concentration and OH exposure: experimental PAM chamber studies, Atmos. Chem. Phys., 11, 1837–1852, doi:10.5194/acp-11-1837-2011, 2011.

Keller-Rudek, H. and Moortgat, G. K.: MPI-Mainz-UV-VIS Spectral Atlas of Gaseous Molecules, Max-Planck-Institut für Chemie, Atmospheric Chemistry Division, www.atmosphere.mpg.de/spectral-atlas-mainz, last access: 7 March 2013.

Keywood, M. D., Varutbangkul, V., Bahreini, R., Flagan, R. C., and Seinfeld, J. H.: Secondary Organic Aerosol Formation from the

Ozonolysis of Cycloalkenes and Related Compounds, Environ. Sci. Technol., 38, 4157–4164, doi:10.1021/es035363o, 2004.

Koppmann, R., Khedim, A., Rudolph, J., Poppe, D., Andreae, M. O., Helas, G., Welling, M., and Zenker, T.: Emissions of organic trace gases from savanna fires in southern Africa during the 1992 Southern African Fire Atmosphere Research Initiative and their impact on the formation of tropospheric ozone, J. Geophys. Res., 102, 18879–18888, doi:10.1029/97jd00845, 1997.

Lambe, A. T., Ahern, A. T., Williams, L. R., Slowik, J. G., Wong, J. P. S., Abbatt, J. P. D., Brune, W. H., Ng, N. L., Wright, J. P., Croasdale, D. R., Worsnop, D. R., Davidovits, P., and Onasch, T. B.: Characterization of aerosol photooxidation flow reactors: heterogeneous oxidation, secondary organic aerosol formation and cloud condensation nuclei activity measurements, Atmos. Meas. Tech., 4, 445–461, doi:10.5194/amt-4-445-2011, 2011.

Lambe, A. T., Onasch, T. B., Massoli, P., Croasdale, D. R., Wright, J. P., Ahern, A. T., Williams, L. R., Worsnop, D. R., Brune, W. H., and Davidovits, P.: Laboratory studies of the chemical composition and cloud condensation nuclei (CCN) activity of secondary organic aerosol (SOA) and oxidized primary organic aerosol (OPOA), Atmos. Chem. Phys., 11, 8913–8928, doi:10.5194/acp-11-8913-2011, 2011b.

Lambe, A. T., Onasch, T. B., Croasdale, D. R., Wright, J. P., Martin, A. T., Franklin, J. P., Massoli, P., Kroll, J. H., Canagaratna, M. R., Brune, W. H., Worsnop, D. R., and Davidovits, P.: Transitions from Functionalization to Fragmentation Reactions of Laboratory Secondary Organic Aerosol (SOA) Generated from the OH Oxidation of Alkane Precursors, Environ. Sci. Technol., 46, 5430–5437, doi:10.1021/es300274t, 2012.

Lee, A., Goldstein, A. H., Kroll, J. H., Ng, N. L., Varutbangkul, V., Flagan, R. C., and Seinfeld, J. H.: Gas-phase products and secondary aerosol yields from the photooxidation of 16 different terpenes, J. Geophys. Res., 111, D17305, doi:10.1029/2006jd007050, 2006.

Lee, T., Sullivan, A. P., Mack, L., Jimenez, J. L., Kreidenweis, S. M., Onasch, T. B., Worsnop, D. R., Malm, W., Wold, C. E., Hao, W. M., and Collett, J. L.: Chemical Smoke Marker Emissions During Flaming and Smoldering Phases of Laboratory Open Burning of Wildland Fuels, Aerosol Sci. Technol., 44, I–V, doi:10.1080/02786826.2010.499884, 2010.

Mao, J., Ren, X., Brune, W. H., Olson, J. R., Crawford, J. H., Fried, A., Huey, L. G., Cohen, R. C., Heikes, B., Singh, H. B., Blake, D. R., Sachse, G. W., Diskin, G. S., Hall, S. R., and Shetter, R. E.: Airborne measurement of OH reactivity during INTEX-B, Atmos. Chem. Phys., 9, 163–173, doi:10.5194/acp-9-163-2009, 2009.

Massoli, P., Lambe, A. T., Ahern, A. T., Williams, L. R., Ehn, M., Mikkilä, J., Canagaratna, M. R., Brune, W. H., Onasch, T. B., Jayne, J. T., Petäjä, T., Kulmala, M., Laaksonen, A., Kolb, C. E., Davidovits, P., and Worsnop, D. R.: Relationship between aerosol oxidation level and hygroscopic properties of laboratory generated secondary organic aerosol (SOA) particles, Geophys. Res. Lett., 37, L24801, doi:10.1029/2010gl045258, 2010.

Matson, P., Lohse, K. A., and Hall, S. J.: The globalization of nitrogen deposition: Consequences for terrestrial ecosystems, Ambio, 31, 113–119, doi:10.1639/0044-7447(2002)031[0113:tgondc]2.0.co;2, 2002.

Matsunaga, A. and Ziemann, P. J.: Gas-Wall Partitioning of Organic Compounds in a Teflon Film Chamber and Potential Effects on Reaction Product and Aerosol Yield Measurements, Aerosol Sci. Technol., 44, 881–892, doi:10.1080/02786826.2010.501044, 2010.

May, A. A., Saleh, R., Hennigan, C. J., Donahue, N. M., and Robinson, A. L.: Volatility of Organic Molecular Markers Used for Source Apportionment Analysis: Measurements and Implications for Atmospheric Lifetime, Environ. Sci. Technol., 46, 12435–12444, doi:10.1021/es302276t, 2012.

McMeeking, G. R., Kreidenweis, S. M., Baker, S., Carrico, C. M., Chow, J. C., Collett Jr., J. L., Hao, W. M., Holden, A. S., Kirchstetter, T. W., Malm, W. C., Moosmüller, H., Sullivan, A. P., and Wold, C. E.: Emissions of trace gases and aerosols during the open combustion of biomass in the laboratory, J. Geophys. Res., 114, D19210, doi:10.1029/2009jd011836, 2009.

Middlebrook, A. M., Bahreini, R., Jimenez, J. L., and Canagaratna, M. R.: Evaluation of Composition-Dependent Collection Efficiencies for the Aerodyne Aerosol Mass Spectrometer using Field Data, Aerosol Sci. Technol., 46, 258–271, doi:10.1080/02786826.2011.620041, 2012.

Molina, M. J., Ivanov, A. V., Trakhtenberg, S., and Molina, L. T.: Atmospheric evolution of organic aerosol, Geophys. Res. Lett., 31, L22104, doi:10.1029/2004gl020910, 2004.

Murphy, D. M., Cziczo, D. J., Froyd, K. D., Hudson, P. K., Matthew, B. M., Middlebrook, A. M., Peltier, R. E., Sullivan, A., Thomson, D. S., and Weber, R. J.: Single-particle mass spectrometry of tropospheric aerosol particles, J. Geophys. Res.-Atmos., 111, D23S32, doi:10.1029/2006jd007340, 2006.

Ng, N. L., Canagaratna, M. R., Zhang, Q., Jimenez, J. L., Tian, J., Ulbrich, I. M., Kroll, J. H., Docherty, K. S., Chhabra, P. S., Bahreini, R., Murphy, S. M., Seinfeld, J. H., Hildebrandt, L., Donahue, N. M., DeCarlo, P. F., Lanz, V. A., Prévôt, A. S. H., Dinar, E., Rudich, Y., and Worsnop, D. R.: Organic aerosol components observed in Northern Hemispheric datasets from Aerosol Mass Spectrometry, Atmos. Chem. Phys., 10, 4625–4641, doi:10.5194/acp-10-4625-2010, 2010.

Ng, N. L., Canagaratna, M. R., Jimenez, J. L., Chhabra, P. S., Seinfeld, J. H., and Worsnop, D. R.: Changes in organic aerosol composition with aging inferred from aerosol mass spectra, Atmos. Chem. Phys., 11, 6465–6474, doi:10.5194/acp-11-6465-2011, 2011a.

Ng, N. L., Canagaratna, M. R., Jimenez, J. L., Zhang, Q., Ulbrich, I. M., and Worsnop, D. R.: Real-Time Methods for Estimating Organic Component Mass Concentrations from Aerosol Mass Spectrometer Data, Environ. Sci. Technol., 45, 910–916, doi:10.1021/es102951k, 2011b.

Park, R. J., Jacob, D. J., and Logan, J. A.: Fire and biofuel contributions to annual mean aerosol mass concentrations in the United States, Atmos. Environ., 41, 7389–7400, doi:10.1016/j.atmosenv.2007.05.061, 2007.

Pope, C. A., Burnett, R. T., Thun, M. J., Calle, E. E., Krewski, D., Ito, K., and Thurston, G. D.: Lung cancer, cardiopulmonary mortality, and long-term exposure to fine particulate air pollution, Jama-Journal of the American Medical Association, 287, 1132–1141, doi:10.1001/jama.287.9.1132, 2002.

Robinson, A. L., Donahue, N. M., Shrivastava, M. K., Weitkamp, E. A., Sage, A. M., Grieshop, A. P., Lane, T. E., Pierce, J. R., and Pandis, S. N.: Rethinking Organic Aerosols: Semivolatile Emissions and Photochemical Aging, Science, 315, 1259–1262, doi:10.1126/science.1133061, 2007.

Spracklen, D. V., Logan, J. A., Mickley, L. J., Park, R. J., Yevich, R., Westerling, A. L., and Jaffe, D. A.: Wildfires drive interannual variability of organic carbon aerosol in the western U.S. in summer, Geophys. Res. Lett., 34, L16816, doi:10.1029/2007gl030037, 2007.

Sueper, D. T., Allan, J., Dunlea, E., Crosier, J., Kimmel, J., DeCarlo, P., Aiken, A. C., and Jimenez, J. L.: A Community Software for Quality Control and Analysis of Data from the Aerodyne Time-of-Flight Aerosol Mass Spectrometers (ToF-AMS), 2007 Annual Conference of the American Association for Aerosol Research, Reno, ND, USA, 2007.

Trost, B., Stutz, J., and Platt, U.: UV-absorption cross sections of a series of monocyclic aromatic compounds, Atmos. Environ., 31, 3999–4008, doi:10.1016/s1352-2310(97)00214-8, 1997.

Van Krevelen, D. W.: Graphical-statistical method for the study of structure and reaction processes of coal, Fuel, 24, 269–284, 1950.

Warneke, C., de Gouw, J. A., Lovejoy, E. R., Murphy, P. C., Kuster, W. C., and Fall, R.: Development of proton-transfer ion trap-mass spectrometry: On-line detection and identification of volatile organic compounds in air, J. Am. Soc. Mass Spectrom., 16, 1316–1324, doi:10.1016/j.jasms.2005.03.025, 2005a.

Warneke, C., Kato, S., De Gouw, J. A., Goldan, P. D., Kuster, W. C., Shao, M., Lovejoy, E. R., Fall, R., and Fehsenfeld, F. C.: Online volatile organic compound measurements using a newly developed proton-transfer ion-trap mass spectrometry instrument during New England Air Quality Study – Intercontinental Transport and Chemical Transformation 2004: Performance, intercomparison, and compound identification, Environ. Sci. Technol., 39, 5390–5397, doi:10.1021/es050602o, 2005b.

Warneke, C., Roberts, J. M., Veres, P., Gilman, J., Kuster, W. C., Burling, I., Yokelson, R., and de Gouw, J. A.: VOC identification and inter-comparison from laboratory biomass burning using PTR-MS and PIT-MS, International J. Mass Spectrom., 303, 6–14, doi:10.1016/j.ijms.2010.12.002, 2011.

Watson, J. G.: Visibility: Science and regulation, J. Air Waste Manage. Assoc., 52, 628–713, 2002.

Yokelson, R. J., Griffith, D. W. T., and Ward, D. E.: Open-path Fourier transform infrared studies of large-scale laboratory biomass fires, J. Geophys. Res., 101, 21067–21080, doi:10.1029/96jd01800, 1996.

Yokelson, R. J., Crounse, J. D., DeCarlo, P. F., Karl, T., Urbanski, S., Atlas, E., Campos, T., Shinozuka, Y., Kapustin, V., Clarke, A. D., Weinheimer, A., Knapp, D. J., Montzka, D. D., Holloway, J., Weibring, P., Flocke, F., Zheng, W., Toohey, D., Wennberg, P. O., Wiedinmyer, C., Mauldin, L., Fried, A., Richter, D., Walega, J., Jimenez, J. L., Adachi, K., Buseck, P. R., Hall, S. R., and Shetter, R.: Emissions from biomass burning in the Yucatan, Atmos. Chem. Phys., 9, 5785–5812, doi:10.5194/acp-9-5785-2009, 2009.

Zhang, Q., Jimenez, J. L., Canagaratna, M. R., Allan, J. D., Coe, H., Ulbrich, I., Alfarra, M. R., Takami, A., Middlebrook, A. M., Sun, Y. L., Dzepina, K., Dunlea, E., Docherty, K., DeCarlo, P. F., Salcedo, D., Onasch, T., Jayne, J. T., Miyoshi, T., Shimono, A., Hatakeyama, S., Takegawa, N., Kondo, Y., Schneider, J., Drewnick, F., Borrmann, S., Weimer, S., Demerjian, K., Williams, P., Bower, K., Bahreini, R., Cottrell, L., Griffin, R. J., Rautiainen, J., Sun, J. Y., Zhang, Y. M., and Worsnop, D. R.: Ubiquity and dominance of oxygenated species in organic aerosols in anthropogenically-influenced Northern Hemisphere midlatitudes, Geophys. Res. Lett., 34, L13801, doi:10.1029/2007gl029979, 2007.